Energy Conversion and Management 227 (2021) 113491

Contents lists available at ScienceDirect

Energy Conversion and Management

journal homepage: www.elsevier.com/locate/enconman

Parameter estimation of photovoltaic models using an improved marine predators algorithm

Mohamed Abdel-Basset [a,*], Doaa El-Shahat [a], Ripon K. Chakrabortty [b], Michael Ryan [b]

[a] Faculty of Computers and Informatics, Zagazig University, Zagazig, Sharqiyah 44519, Egypt
[b] Capability Systems Centre, School of Engineering and IT, UNSW Canberra, Australia

ARTICLE INFO

Keywords:
Parameter estimation
Photovoltaic model
Marine predators algorithm
Solar energy

ABSTRACT

The abundance of solar energy as one of the clean energy forms offers a great advantage as an alternative to non-renewable energy sources. The photovoltaic system is a promising technology that directly converts sunlight into a direct current. Parameter estimation of photovoltaic systems is a challenging task that has a significant influence on the efficiency of these systems. Most of the existing methods employed for identifying parameters of photovoltaic systems suffer from high computing burdens, fall into local optima, or struggle with the intricate adjustment required of the algorithm parameters to provide the best performance. This paper, therefore, proposes an improved algorithm based on the new metaheuristic marine predators algorithm to extract the optimal values of photovoltaic parameters. The improved marine predators algorithm employs a population improvement strategy to enhance the quality of the solutions by utilizing two different ways to handle the solutions inside the population-based on the population mean fitness. The location of a high-quality solution is improved using an adaptive mutation operation, while the location of a low-quality solution is updated according to the location of the best-obtained solution and the location of a good solution selected from the population. A good solution is chosen from the first half of the population after sorting its solutions in ascending order. The results of several experiments show the superior performance of the proposed algorithm compared to existing algorithms on a range of photovoltaic models. The results show that the proposed algorithm is highly correlated with the measured current–voltage data so that it can offer a useful alternative for parameter estimation of photovoltaic models.

1. Introduction

Energy plays an indispensable role in a wide range of sectors, such as manufacturing, agriculture, transportation, and housing. Recently, there has been a tremendous increase in global energy consumption. Although fossil fuels have been a significant source of energy production for many decades, their prices are steadily increasing and the possibility of exhaustion means that they are an unsustainable source of energy. Fossil fuels such as coal, oil, and natural gas also contain high levels of carbon so that carbon emission from their combustion is the most significant contributor to global warming, which threatens life on Earth [1]. Consequently, renewable and clean energy sources –such as wind, wave, biomass, and sunlight—are sought as safe, abundant, and environmentally friendly sources of energy.

Solar energy is the second most common renewable source of energy after wind [2] and is one of the most promising energy sources that has spread to include many applications such as water heating [3,4], street lightening [5,6], vehicles [7–9], solar farming [10], tourism [11], irrigation [12–14]. Solar energy is turned into a useful source of electricity with the help of the photovoltaic (PV) system based on the building block of the solar cell that converts the absorbed sunlight into Direct Current (DC) which, through an inverter, is then converted to Alternating Current (AC).

PV systems have a wide variety of configurations, including standalone (off-grid), grid-connected (tied-grid), and hybrid systems. The standalone system operates independently from the electric distribution grid and requires battery storage to ensure that electricity is continuously available. Such a system is suitable for television, phone signals, marines, homes, billboards, street lighting, and rural clinics. The grid-connected system is coupled with an electric distribution grid for

* Corresponding author.
E-mail addresses: mohamed.abdelbasset@fci.zu.edu.eg (M. Abdel-Basset), doaaelshahat@zu.edu.eg (D. El-Shahat), r.chakrabortty@adfa.edu.au (R.K. Chakrabortty), m.ryan@adfa.edu.au (M. Ryan).

https://doi.org/10.1016/j.enconman.2020.113491
Received 12 May 2020; Received in revised form 28 September 2020; Accepted 29 September 2020
Available online 27 October 2020

Table 1
Review of the existing metaheuristic algorithms for parameter extraction of PV models.

Algorithm	Year	PV Model	Summary
Classified Perturbation Mutation Based PSO Algorithm (CPMPSO) [34]	2020	SDM, DDM, and PV modules	- The Classified Perturbation Mutation Strategy (CPMS) is introduced to CPMPSO. - CPMPSO is an effective and stable algorithm. - CPMPSO consumes time due to the CPMS.
Enhanced Adaptive Differential Evolution (EJADE) [35]	2020	SDM, DDM, and PV modules	- EADE incorporates the crossover sorting mechanism to transfer good elements to the next generation. - A dynamic population reduction strategy improves the convergence speed. - EJADE is applied for parameter estimation for both experimental and manufacturer datasheet.
Harris hawks optimization (HHO) [63]	2020	TDM	- HHO is time-saving. - HHO estimates only five parameters. - Derived equations to compute the other four parameters. - HHO needs to be applied to other different PV models.
Grasshopper Optimization Algorithm (GOA) [64]	2020	TDM, and two commercial PV modules (Kyocera KC200GT and Solarex MSX-60)	- GOA needs comparisons with more algorithms. - It requires more statistical analysis, such as time.
Whale Optimization Algorithm based Reflecting Learning (RLWOA) [65]	2020	SDM	- It would be better to test RLOWA with different PV models. - RLWOA lacks time analysis.
Improved Electromagnetism-like (IEM) algorithm [66]	2020	SDM	- The nonlinear equation is added to IEM. - Simplifying the total force formula to accelerate the search for the optimal solution.
Salp Swarm Algorithm (SSA) [67]	2020	SDM, DDM	- SSA takes into account the measurement uncertainty parameter to estimate the parameters for SDM and DDM.
Grey Wolf Optimizer And Cuckoo Search (GWOCS) [68]	2020	SDM, DDM, and PV modules	- GWOCS used new opposition - learning strategy.
Biogeography-based Heterogeneous Cuckoo Search(BHCS) [69]	2019	SDM, DDM, and PV modules	- The efficacy of BHCS is attributed to the combination of cuckoo search and biogeography algorithms.
Improved Teaching-Learning-Based Optimization (ITLBO) [70]	2019	SDM, DDM, and PV modules	- ITLBO is incorporated with a new learning strategy in the learning phase. - The teacher in ITLBO presents a different teaching way of guiding the learners.
Performance-Guided JAYA (PGJAYA) [71]	2019	SDM, DDM, and PV modules	- PGAYA adopts self-adaptive chaotic perturbation to improve the population. - The individual performance is quantified by a probability.
Modified Flower Algorithm (MFA) [72]	2019	SDM, DDM, and PV module manufacturer data	- MFA shows better accuracy compared to other algorithms.
Multiple Learning Backtracking Search Algorithm (MLBSA) [73]	2018	SDM, DDM, and PV module	- MLBSA used an elite method based on a local search to ameliorate the population. - MLBSA has a high running time.
Bee pollinator Flower Pollination Algorithm (BPFPA) [74]	2017	SDM and DDM	- BPFPA combines the artificial bee colony algorithm with the flower pollination algorithm. - The bee behaviors are employed at the initial stages of BPFPA.
Generalized Oppositional Teaching Learning-Based Optimization (GOTLBO) [75]	2016	SDM and DDM	- GOTLBO employs opposition-based learning to the teaching learning-based optimization algorithm. - The accuracy is degraded when compared with other algorithms like Rcr-IJADE and STLBO [76,77].
Time-Varying Acceleration Coefficients PSO (TVACPSO) [78]	2016	SDM, DDM, and PV module	- The personal coefficient is decreasing during iterations, whole the social coefficient is increasing. - TVACPSO handled the premature convergence caused by the standard PSO.
Differential Evolution with Integrated Mutation per iteration (DEIM) [79]	2015	DDM	- DEIM applies the attraction–repulsion idea of the electromagnetism-like algorithm to improve the mutation operation of the conventional DE. - DEIM uses the sigmoid function to automatically tune the mutation scaling and the crossover rate based on the current and previous fitness. - DEIM needs to be applied to other different PV models

immediate utilization or sale back through the grid to electricity supply companies. The hybrid system is a grid-connected system with battery storage. PV systems vary in design, technology, size, and location, which may result in a difference in energy production or loss [15].

Generally, various types of PV cells are made according to the form of the used silicon, such as mono-crystalline [16], poly-crystalline [17], and amorphous thin-film [18]. Each type of PV cell has different manufacturing procedures, constituent material, cost, and efficiency. Silicon is widely used in solar photovoltaic cells because of its abundance, and its physical properties are well-studied [19,20]. The mono-crystalline solar cell has the highest efficiency (about 17%-25%) [21] but is expensive due to the waste of the silicon material to cut the four sides during the manufacturing process [22]. Mono-crystalline silicon is also space-efficient and has the most prolonged operating period. In contrast, poly-crystalline is less efficient (about 12%-18%) [21] due to the recombination of several grain boundaries [23], but its manufacturing cost is lower and it is easier to produce. Amorphous thin-film cells have the advantage of being more cost-effective [24], but they are less efficient than crystalline silicon cells.

The main challenge is to optimize the PV system efficiency during operation by the use of an accurate model based on the measured current–voltage data. Although manufacturers validate the current–voltage curve under Standard Test Conditions (STC)—solar irradiance = 1000 W/m^2, temperature = 25 °C, and air mass = 1.5 AM—the efficiency of the PV system may be substantially affected by external environment changes in irradiance, temperature, and atmospheric pressure. Various PV models have therefore been developed, such as the Single Diode Model (SDM), new one-diode model [25], Double-Diode Model (DDM), improved two-diode model [26], modified double-diode model [27], simplified two-diode model [28], and Three-Diode Model (TDM) [29].

These models vary whether in the accuracy or the complexity of their equivalent circuits, with the single-diode and double-diode models being the most commonly adopted models. Generally, the accuracy of the PV system relies on its model parameters so the identification and estimation of those parameters are necessary to improve the efficiency of the system.

Consequently, researchers have sought to optimize the behavior of the PV system through various design methods, which can be categorized into analytical, deterministic, and metaheuristic methods. The analytical approaches [30–33] employ a set of mathematical equations to identify the values of the unknown parameters. Despite the ease of implementation and speed of obtaining results, the analytical methods can be inaccurate and result in a major difference between the simulated and the measured performance of the actual PV model depending on some assumptions that are made in advance under STC [34,35]. Deterministic methods require constraints on the model, including convexity and differentiability—Lambert W-functions [36], iterative approach [37], and the Newton-Raphson method [38] are examples. The parameter extraction of the PV model is a non-linear and multi-modal problem, which makes the deterministic methods fall into local optima and may result in low efficiency if the initial points are away from the global optimal [35,39].

Metaheuristics are considered a promising alternative for the PV parameter estimation problem to overcome the shortcomings of the aforementioned methods. Additionally, they can balance between the exploration and the exploitation phases to avoid stagnation in local optima. Several metaheuristic algorithms have recently emerged to address problems such as scheduling [40], economic dispatch problems [41], resource allocation [42], optimal power flow [43], knapsack problem [44], and feature selection [45]. The remarkable superiority of the *meta*-algorithms, as well as the importance of solar energy and its sweeping of many practical applications, motivated this work to propose a new metaheuristic algorithm to estimate parameters of PV models.

Various metaheuristics have been applied for accurate parameter identification of different PV models [46–48]. Alam et al. [49] suggested the flower pollination algorithm to extract the optimal parameters of the single diode and double diode models. Furthermore, bacterial foraging algorithm [50] was introduced with new equations to derive the values of open-circuit voltage and voltage at maximum power that help to precisely predict the solar PV characteristics. Chen et al. [51] hybridized the bee colony optimization algorithm with the teaching–learning-based optimization algorithm to ameliorate the accuracy of the single metaheuristic algorithms.

Ishaque et al. [52] presented the Differential Evolution (DE) which can measure the model parameters for many types of PV models (monocrystalline, multi-crystalline, and thin-film) at different irradiance and temperature. In [53], DE was employed with a penalty function to bring the values of the parameters back into the feasible range after performing the crossover. Biswas et al. [54] proposed the L-SHADE algorithm that adapts its parameters (the crossover rate and the scaling factor) based on the success history of these parameters in the previous generations. L-SHADE adopts a linear function that dynamically lessens the size of the population. In [55], in addition to the success history of the adaptive DE, the Nelder-Mead simplex method is incorporated to enhance the solution and the ranking-based elimination strategy was employed to keep the promising solutions in an external archive.

Jordehi [56] overcame the premature convergence of Particle Swarm Optimization (PSO) by adopting the idea of an enhanced leader. The enhanced leader is improved with a five-stage successive mutation and affects the collective performance of the particles. In [57], the performance of PSO is supported by the mutation operation that depends on the current iteration. The sine cosine algorithm is combined with the Nelder-Mead simplex approach and the opposition-based learning scheme [58]. In the case of the moth search algorithm [59], the disruptor operator is employed for avoiding the local optima. Furthermore, the cuckoo search algorithm is another metaheuristic algorithm is applied for estimating the optimal parameters of PV models [60,61]. The authors [62] added the opposition–based learning scheme to the sine cosine algorithm.

A number of these recent algorithms are reviewed in Table 1.

Although many of these algorithms are efficient, they may require tuning of several parameters through several experiments or through trial and error, which can take a lot of time. Some algorithms need to test their efficacy and performance on the different models of PV and need to be compared to more robust and recent algorithms to prove their effectiveness. Also, the employed searching strategy may result in an inaccurate extraction of the parameters and may consume much time. The proposed algorithm IMPA comes to handle the aforementioned shortcomings faced by the algorithms as the results show the superiority of IMPA in obtaining high accuracy for the different models in a reasonable time. IMPA has a high convergence speed toward the global optimal and doesn't need to train its parameters.

The Marine Predators Algorithm (MPA) is a new metaheuristic algorithm that has shown high performance in solving real-world engineering problems [80]. This paper presents the design of an Improved Marine Predators Algorithm (IMPA) that can accurately optimize the parameters of different PV models. Based on the mean fitness of the population, IMPA develops a Population Improvement Strategy (PIS) that splits solutions into two categories based on the mean fitness of this population, each of which is dealt with a different way to enhance the quality of the solutions. For high-quality solutions, we adopt an adaptive mutation operation in which a random position is selected from this solution, and its value is replaced with another value generated randomly between the lower and upper bounds of this chosen parameter and it is updated in the population if it is better the old solution. We update the low-quality solution based on the location of the top predator and a good-quality predator chosen from the first half of the population after sorting the solutions according to their fitness. Indeed, the PIS accelerates the convergence speed of the population toward the global optimum solution. The main contributions of the paper are as follows:

- IMPA is proposed to accurately estimate PV model parameters.
- An effective strategy called PIS is employed to refine the quality of the solutions.
- The efficacy of IMPA is tested in comparison with the other existing algorithms using different PV models (SDM, DDM, and PV module) for both the benchmark data and from the manufacturer's datasheet.
- The results of several experiments and statistical analyses prove the superiority of IMPA.

The remainder of this paper is organized as follows. Section 2 presents the problem formulation of PV models and section 3 introduces the standard MPA. Section 4 presents the proposed improved MPA for parameter estimation of PV models. Section 5 contains the experimental results and analysis of different PV models. Moreover, section 6 introduces the managerial implications of our proposed work. Finally, section 7 concludes and identifies some future work.

2. Problem formulation

SDM and DDM are the most widespread of various models used to illustrate the current–voltage characteristics of solar cells employing diodes. These models have different parameters to be estimated and optimized and environmental changes, as well as nonlinear behaviors and aging of the solar cells, mean that these parameter values change over time. The following subsections describe these models and present the photovoltaic module.

2.1. Solar cell models

2.1.1. Single-diode model

Due to its simplicity and easy implementation, the SDM is the most

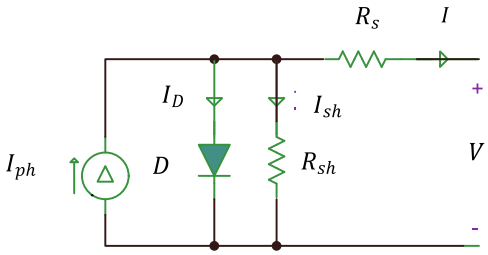

Fig. 1. The equivalent circuit for the single-diode model.

adopted used model. Fig. 1 shows the equivalent circuit of the SDM which consists of a current source connected with parallel with a diode in addition to two resistors. The mathematical model of the cell output current I SDM is:

$$I = I_{ph} - I_D - I_{sh} \tag{1}$$

$$I_D = I_{Rd}\left(exp\left(\frac{V + I^*R_s}{n^*V_t}\right) - 1\right) \tag{2}$$

$$I_{sh} = \frac{V + I^*R_s}{R_{sh}} \tag{3}$$

$$V_t = \frac{k^*T}{q} \tag{4}$$

where $I_{ph}$and $I_D$represent the photo-generated current and the diode current, respectively. I_{sh}refers to the current of the shunt resistor. $I_D$is calculated using Eq. (2), where I_{Rd} determines the reverse saturation current of the diode.V denotes the output voltage and V_t indicates the junction thermal voltage. n represents the ideality factor of the diode, and R_s represents the series resistance. k is the Boltzmann constant: $1.3806503 \times 10^{-23}$J/K. $q = 1.60217646 \times 10^{-19}$C which is the electron charge and T is the temperature in Kelvin. By combining and substituting Eqs. (2–4) in Eq. (1), the output current can be rewritten as:

$$I = I_{ph} - I_{Rd}\left(exp\left(\frac{q^*(V + I^*R_s)}{n^*k^*T}\right) - 1\right) - \frac{V + I^*R_s}{R_{sh}} \tag{5}$$

where I and V are the measured data previously determined by the manufacturer and the values of q, k, and T are given. There are therefore five unknown parameters that need to be estimated and optimized (I_{ph}, I_{Rd},n,R_s,R_{sh}). The identification of the parameters is a challenging task as it has a significant influence on the performance and accuracy of the solar cell.

2.1.2. Double-diode model

Despite the simplicity of the SDM, it is inaccurate in low illumination. In contrast, the DDM [81] is more accurate and better describes the behaviors of the solar cell, even in limited light. However, the DDM is more computationally complicated with more parameters since it considers recombination losses. Fig. 2 shows an equivalent circuit for DDM, which contains two diodes connected in parallel with a current source, shunt resistance, and series resistance. The output current I generated from the DDM is:

$$I = I_{ph} - I_{D1} - I_{D2} - I_{sh} \tag{6}$$

where I_{D1} and I_{D2} are the current of the first and the second diode and calculated as follows:

$$I_{D1} = I_{Rd1}\left(exp\left(\frac{V + I^*R_s}{n_1^*V_t}\right) - 1\right) \tag{7}$$

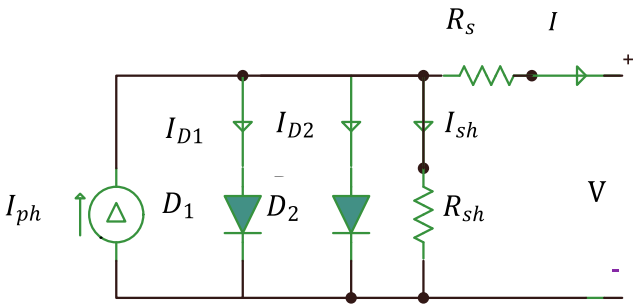

Fig. 2. The equivalent circuit for the double-diode model.

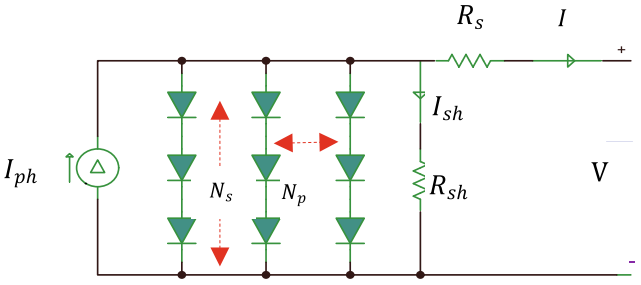

Fig. 3. The equivalent circuit for the PV module.

$$I_{D2} = I_{Rd2}\left(exp\left(\frac{V + I^*R_s}{n_2^*V_t}\right) - 1\right) \tag{8}$$

I_{Rd1} and I_{Rd2} are the reverse saturation current of the first and the second diodes. $n_1$and n_2 are the ideality factors of the two diodes.

Then, the mathematical equation for expressing output current of DDM is as follows:

$$I = I_{ph} - I_{Rd1}\left(exp\left(\frac{V + I^*R_s}{n_1^*V_t}\right) - 1\right) - I_{Rd2}\left(exp\left(\frac{V + I^*R_s}{n_2^*V_t}\right) - 1\right) - \frac{V + I^*R_s}{R_{sh}} \tag{9}$$

As can be seen in Eq. (9) there are seven unknown parameters to be estimated: including I_{ph}, I_{Rd1}, I_{Rd2}, R_s, R_{sh}, n_1, and n_2.

2.2. Photovoltaic module model

As is evident in Fig. 3, the equivalent circuit of the Photovoltaic (PV) module model is more intricate because it incorporates more solar cells connected in series and/or parallel. The output current of the PV module is expressed as follows [70]:

$$I = I_{ph}^*N_p - I_{Rd}^*N_p\left(exp\left(\frac{V + \frac{I^*R_s^*N_s}{N_p}}{n_1^*N_s^*V_t}\right) - 1\right) - \frac{V + \frac{I^*R_s^*N_s}{N_p}}{\frac{R_{sh}^*N_s}{N_p}} \tag{10}$$

N_s indicates the number of the solar cells connected in series, while N_p indicates the number of solar cells connected in parallel. It is common to use the single diode solar cells in the PV module that are connected in series [82]. In our experiments, since the solar cells are connected in series for the used PV module model, N_p is set to 1. Hence, Eq. (10) can be simplified as follows [35,82,83]:

$$I = I_{ph} - I_{Rd}\left(exp\left(\frac{V + I^*R_s^*N_s}{n_1^*N_s^*V_t}\right) - 1\right) - \frac{V + I^*R_s^*N_s}{R_{sh}^*N_s} \tag{11}$$

From Eq. (11), the PV model requires estimating the same five unknown parameters (I_{ph},I_{Rd},n,R_s,R_{sh}) as SDM.

3. Marine predators algorithm

Faramarzi et al. [80] developed a new algorithm called the marine predators algorithm that mimics the life of marine predators and their prey using three phases. These steps describe the predator step size while catching the prey and summarized as follows:

- ***Phase 1***: In high-velocity ratio (V≥10), the predator moves faster than the prey. This phase occurs in the first third of iterations in the exploration phase, The mathematical model of this phase is:

$$\overrightarrow{prey_i} = \overrightarrow{prey_i} + P.\overrightarrow{Rand_B} \otimes \overrightarrow{stepsize_i} if t < \frac{Max\_T}{3} \tag{12}$$

$$\overrightarrow{Stepsize} = \overrightarrow{Rand_B} \otimes \left(\overrightarrow{Elite_i} - \overrightarrow{Rand_B} \otimes \overrightarrow{prey_i}\right), i = 1, \cdots, N \tag{13}$$

$$\overrightarrow{Rand_B} = \frac{1}{\sqrt{2\pi}} \exp\left(\frac{-x^2}{2}\right) \tag{14}$$

where R is a vector containing random numbers ∈ [0, 1]. The notation ⊗ is entry-wise multiplications and $P = 0.5$. Max_T is the maximum course of iterations, t refers to the current iteration, and N determines the size of the population. $\overrightarrow{Rand_B}$ is a vector of random numbers generated from the Brownian motion that draws the step length from a normal distribution with a mean of zero and unit variance of 1. $\overrightarrow{Elite_i}$ is a matrix that contains the fittest solution which is recommended as a top predator. Using this motion, we can calculate the probability density function (PDF) at a point x as described in Eq. (14).

- ***Phase 2***: In the unit velocity ratio (V≈1), the predator and the prey move at the same speed. It is the intermediate phase where the prey employs the exploration using Lévy distribution and the predator employs the exploitation using Brownian motion. Therefore, the algorithm uses the first half of the population for exploration, while the other half is for exploitation. We update the prey movement by the Lévy distribution as follows:

$$\overrightarrow{prey_i} = \overrightarrow{prey_i} + P.\overrightarrow{Rand_L} \otimes stepsize_i, \mathrm{i} = 1, \cdots, \mathrm{N}/2 if \frac{Max\_T}{3} < t < \frac{2*Max\_T}{3} \tag{15}$$

$$\overrightarrow{Stepsize} = \overrightarrow{Rand_L} \otimes \left(\overrightarrow{Elite_i} - \overrightarrow{Rand_L} \otimes \overrightarrow{prey_i}\right) \tag{16}$$

$$z = 0.05 \times \frac{Q}{|Y|^{1/\propto}}, Q\ N(0, \sigma^2), Y\ Normal(0, 1) \tag{17}$$

$$\sigma^2 = \left[\frac{\Gamma(1+\propto)*sin\frac{\pi\propto}{2}}{\propto*\Gamma\left(\frac{1+\propto}{2}\right)*2^{\frac{\propto-1}{2}}}\right]^{1/\propto}, \propto = 1.5 \tag{18}$$

$$\overrightarrow{Rand_L} = \frac{\gamma\Gamma(1+\propto)\sin(\frac{\pi\propto}{2})}{\pi z^{(1+\propto)}} \tag{19}$$

where Q and Y are two random numbers drawn from the normal distribution, σ^2 is the variance, and$\propto = 1.5$ and z determines the step size calculated using Gaussian distributions through generating two random numbers Q and Y. $\overrightarrow{Rand_L}$is a vector of random numbers generated from the Lévy distribution of the Mantegna method [84]. We update the predator movement by Brownian motion using the other half of the population:

$$\overrightarrow{prey_i} = \overrightarrow{prey_i} + P.CF \otimes stepsize_i, \mathrm{i} = \mathrm{N}/2, \cdots, Nif \frac{Max\_T}{3} < t < \frac{2*Max\_T}{3} \tag{20}$$

$$\overrightarrow{Stepsize} = \overrightarrow{Rand_B} \otimes \left(\overrightarrow{Elite_i} - \overrightarrow{Rand_B} \otimes \overrightarrow{prey_i}\right) \tag{21}$$

$$CF = (1 - \frac{t}{Max\_T})^{(2*\frac{t}{Max\_T})} \tag{22}$$

where CF is an adaptive parameter to control the step size of the predator motion.

- ***Phase 3***: In low-velocity ratio (V = 1), the predator moves faster than the prey using the Lévy in the last third of iterations and mathematically formulated as:

$$\overrightarrow{prey_i} = \overrightarrow{Elite_i} + P.CF \otimes stepsize_i, \mathrm{i} = 1, \cdots, nift > \frac{2*Max\_T}{3} \tag{23}$$

$$\overrightarrow{Stepsize} = \overrightarrow{Rand_L} \otimes \left(\overrightarrow{Rand_L} \otimes -\overrightarrow{Elite_i} - \overrightarrow{prey_i}\right) \tag{24}$$

The eddy formation or Fish Aggregating Devices (FADs) can affect the behavior of the marine predators. The mathematical model of the FADS effect is:

$$\overrightarrow{prey_i} = \begin{cases} \overrightarrow{prey_i} + CF\left[\overrightarrow{X_{min}} + \overrightarrow{R} \otimes (\overrightarrow{D_{max}} - \overrightarrow{D_{min}}) \otimes \overrightarrow{B}\right] ifr \le FADs \overrightarrow{prey_i} + [FADs(1-r) + r](\overrightarrow{prey_{rand1}} - \overrightarrow{prey_{rand2}}) ifr > FADs \end{cases} \tag{25}$$

where FADs = 0.2 and it is the probability of the FADs effect on the optimization process. $\overrightarrow{B}$ is a binary vector containing arrays of 0 and 1, which is constructed by generating a random vector belongs to [0, 1]. The array will be zero if its value less than FADs; otherwise, the array will be one. $\overrightarrow{D_{max}}$ and $\overrightarrow{D_{min}}$ is the upper and lower bounds of the dimension. *rand*1 and *rand*2 two random indices within the prey matrix. The memory saving in MPA simulates the good memory of the marine predators to remember the locations where they succeed in catching their prey. Therefore, MPA updates the Elite matrix after updating the Prey matrix and the FADs effect. This process supports the quality of the solutions. Algorithm 1 presents the pseudocode of the standard MPA.

Algorithm 1 The standard MPA

1. Initialize search agents or the *prey* population $i = 1, \cdots, N$
2. $t = 1$
3. **while** $(t < Max\_T)$
4. Calculate the fitness and create the *Elite* matrix
5. **if** $(t < \frac{Max\_T}{3})$
6. Update prey using Eq. (12)
7. **else if** $(\frac{Max\_T}{3} < t < \frac{2*Max\_T}{3})$
8. **for** $i = 1 : \frac{N}{2}$
9. Update prey based on Eq. (15)
10. **for** $i = \frac{N}{2} : N$
11. Update prey based on Eq. (20)
12. **else if** $(t > \frac{2*Max\_T}{3})$

(*continued on next page*)

(*continued*)

Algorithm 1 The standard MPA

13. Update prey based on Eq. (23)
14. **end if**
15. Achieve memory saving and update Elite matrix
16. Apply the FADs effect and update using Eq. (25)
17. Accomplish memory saving and update Elite matrix
18. **end while**

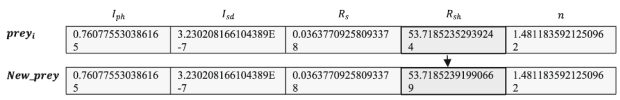

Fig. 4. An illustration of the adaptive mutation operation used by the proposed algorithm.

4. The proposed algorithm

In this section, we are interested in illustrating the main idea of the proposed algorithm of Improved MPA (IMPA) for estimating the unknown parameters of the PV system. As mentioned earlier, MPA is a new metaheuristic algorithm that has proven performance in tackling real-world engineering problems [80]. Accordingly, we suggest using MPA for optimizing the unknown parameters of the PV system. Furthermore, we have introduced a new technique to enhance the reliability of the MPA and its capacity to address this problem called the Population Improvement Strategy (PIS), which increases the quality of solutions in the population. The next subsection presents the main stages that form the IMPA, including initialization, objective function, and the PIS.

4.1. Initialization

The proposed algorithm initializes a population *prey* as a set of randomly generated N predators or solutions. Each solution has a dimension D that determines the number of the variables or the unknown parameters for each PV model. For example, in the SDM and PV module, $D = 5$; while $D = 7$ for the DDM. We generate each parameter that has a lower bound Y_{min} and an upper bound Y_{max} using the following equation:

$$prey_{i,j} = Y_{min} + r^*(Y_{max} - Y_{min}), i = 1, \cdots, N, j = 1, \cdots, D \tag{26}$$

$prey_{i,j}$ represents the j^{th} parameter of a solution numbered i in the population, and r is a random number $\in[0, 1]$. Hence, to construct the *Elite* matrix, we replicate the top predator N times. The top predator is the solution that has the minimum fitness function value. The next subsection explains how to evaluate the solutions in the population.

4.2. Objective function

The parameter estimation of the PV system is treated as an optimization problem to minimize the error between the simulated data and the measured data. Accordingly, we use the root mean square error (RMSE) to determine the error between the simulated current and the measured current. Given the measured current–voltage (I-V), each predator $prey_i$ in the initial population is evaluated using RMSE that is widely employed in literature [34,67–69,85,86] for each PV model as follows:

$$RMSE(prey_i) = \sqrt{\frac{1}{M}^* \sum_{k=1}^{M} F_k(I, V, prey_i)} \tag{27}$$

where $F_k(I, V, prey_i)$ denotes the error for each k^{th} pair of the simulated and the measured current data. M is the length of the measured data.

4.3. Population improvement strategy

The population improvement strategy promotes the quality of any solution within the population by comparing its fitness to the mean fitness of this population (*Mean_fit*), and is calculated as follows:

$$Mean\_fit = \frac{1}{N}^* \sum_{i=1}^{N} fitness_i \tag{29}$$

where $fitness_i$ represents the fitness of the i^{th} prey. The mean fitness splits the population into two categories of high-quality solutions and low-quality solutions. High-quality solutions have fitness lower than the mean fitness, while low-quality solutions have fitness higher than the mean fitness. To enhance the quality of each solution, a different strategy is followed for each category.

For high-quality solutions, the adaptive mutation operation is adopted with a probability of 0.5 to reduce the time burden. When we increase the mutation probability, the results have no more changes. In the mutation operation, a random position is selected from the solution, and its value is replaced with another value generated randomly between the lower and upper bounds of this chosen parameter as shown in Fig. 4. *New_prey* is the new mutated solution and is replaced with the solution in the population if it is better.

For the low-quality solutions, we update this solution based on the location of the top predator and a good-quality predator chosen from the first half of the population after sorting the solutions according to their fitness.

$$New\_prey_j = \frac{Top\_predator_j + prey\_Rand_{loc,j}}{2}, j = 1, \ldots, D, loc = rand \in [1, N/2] \tag{30}$$

loc is the index of a randomly selected predator from the first half of the prey population. The PIS boosts the fitness of the solutions based on the mean fitness per iteration. Algorithm 2 presents the pseudocode of the proposed algorithm. Additionally, Fig. 5 shows the flowchart of the proposed algorithm IMPA. From the figure, we can see that per iteration we perform the following:

- The PIS is applied to refine the solutions.
- The top predator is updated.

$$F_k(I, V, prey_i) = \begin{cases} I_{ph} - I_{Rd}\left(exp\left(\frac{q^*(V + I^*R_s)}{n^*k^*T}\right) - 1\right) - \frac{V + I^*R_s}{R_{sh}} - IforSDM \\ I_{ph} - I_{Rd1}\left(exp\left(\frac{V + I^*R_s}{n_1{}^*V_t}\right) - 1\right) - I_{Rd2}\left(exp\left(\frac{V + I^*R_s}{n_2{}^*V_t}\right) - 1\right) - \frac{V + I^*R_s}{R_{sh}} - IforDDM \\ I_{ph} - I_{Rd}(exp\left(\frac{V + I^*R_s{}^*N_s}{n_1{}^*N_s{}^*V_t}\right) - 1) - \frac{V + I^*R_s{}^*N_s}{R_{sh}{}^*N_s} - IforPVmodule \end{cases} \tag{28}$$

- The number of iterations is divided into three equal parts, and in each part, the prey matrix is updated using a different equation.
- The memory saving is achieved and the Elite matrix is updated
- The FADs effect is applied and memory saving is accomplished to update the Elite matrix.

By the end of these iterations, the top predator is returned.

Algorithm 2 The proposed IMPA

1. Initialize search agents or the *prey* population $i = 1, \cdots, N$
2. $t = 1$
3. **while** $(t < Max\_T)$
4. Calculate the fitness of each $prey_i$ using Eq. (27)
5. Find *Top_prdator* that has the minimum fitness and construct the *Elite* matrix
6. Calculate the mean fitness of the population using Eq. (29)
7. Sort the *prey* matrix according to their fitness in ascending order
8. **for** $i = 1 : N$
9. **if** $(fitness(prey_i) < Mean\_fit)$
10. // Apply the mutation operation to $prey_i$ better than *Mean_fit*
11. **if** $(rand < 0.5)$
12. Create a vector *Mutated_prey* and copy the contents of $prey_i$ to it
13. Select a *Rand_pos* from *Mutated_prey*
14. $Mutated\_prey_{Rand\_pos} = Y_{min} + r^*(Y_{max} - Y_{min})$
15. **if** $(fitness(Mutated\_prey) < fitness(prey_i))$
16. $prey_i = Mutaed\_prey$
17. Update $fitness(prey_i) = fitness(Mutated\_prey)$
18. **end if**
19. **end if**
20. **else**
21. // Apply Eq. (30) if $prey_i$ that has fitness equal or worse than Mean_fit
22. Create *New_prey* vector
23. Select a $Rand\_prey_i$ from the first half of the *prey*
24. **for** $j = 1 : D$
25. Update *New_prey* using Eq. (30)
26. **if** $(fitness(New\_prey) < fitness(prey_i))$
27. $prey_i = New\_prey$
28. Update $fitness(New\_prey) = fitness(prey_i)$
29. **end if**
30. **end for**
31. Sort the population according to their fitness in ascending order and update *Mean_fit*
32. **end if**
33. **end for**
34. Update the *Top_prdator*
35. **if** $(t < \frac{Max\_T}{3})$
36. Update prey using Eq. (12)
37. **else if** $(\frac{Max\_T}{3} < t < \frac{2*Max\_T}{3})$
38. **for** $i = 1 : \frac{N}{2}$
39. Update prey based on Eq. (15)
40. **for** $i = \frac{N}{2} : N$
41. Update prey based on Eq. (20)
42. **else if** $(t > \frac{2*Max\_T}{3})$
43. Update prey based on Eq. (23)
44. **end if**
45. Achieve memory saving and update Elite matrix
46. Apply the FADs effect and update using Eq. (25)
47. Accomplish memory saving and update Elite matrix
48. t++
49. **end while**

5. Experimental results and discussion

This section is concerned with testing the efficacy of the proposed algorithm IMPA by conducting several experiments using five experimental benchmarks of three PV models (SDM, DDM, and PV module) in addition to another two commercial models. Furthermore, IMPA performance is compared with the other existing modern and robust algorithms for identifying the values of parameters of the different PV models to minimize the error between the measured and the simulated data. All the algorithms are encoded in Java and run on a laptop with the following specifications: Intel(R) Core(TM) i7-4810MQ CPU @ 2.80 GHz, with 16.0 GB memory in Windows 10 with a 64-bit operating system.

Table 2
Ranges of each parameter for different PV models.

Parameter	SDM/DDM		Photowatt-PWP201		STM6-40/36		STP6-120/36	
	LB	UB	LB	UB	LB	UB	LB	UB
I_{ph}(A)	0	1	0	2	0	2	0	8
I_{sd}, I_{sd1}, I_{sd1} (A)	0	1×10^{-6}	0	50×10^{-6}	0	50×10^{-6}	0	50×10^{-6}
$R_s(\Omega)$	0	0.5	0	2	0	36	0	0.36
$R_{sh}(\Omega)$	0	100	0	2000	0	1000	0	1500
n, n_1,n_2	1	2	1	50	1	60	1	50

5.1. Dataset description

This subsection describes the used benchmarks employed for investigating the performance of the algorithms in our various experiments. The five experimental test examples are SDM, DDM, Photowatt-PWP201, STM6-40/36, and STP6-120/36, belonging to three PV

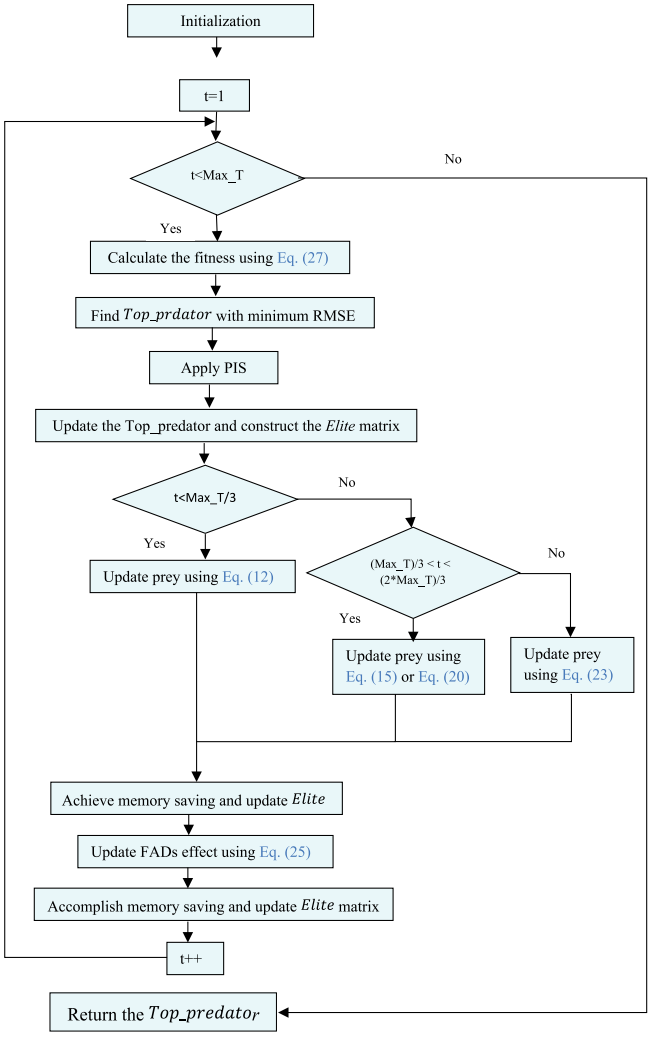

Fig. 5. Flowchart of the proposed algorithm IMPA.

Table 3
Ranges of each parameter for PV commercial models.

Parameter	Mono-crystalline SM55 and thin-film ST40	
	LB	UB
I_{ph}(A)	0	$2*I_{sc}$
I_{sd}	0	100×10^{-6}
$R_s(\Omega)$	0	2
$R_{sh}(\Omega)$	0	5000
n, n_1,n_2	1	4

models. For SDM and DDM, the measured current–voltage data are adopted from [38], which are taken using a 57 mm diameter commercial silicon solar cell under a temperature of 33 °C and solar irradiance of 1000 W/m^2. For the PV module, we employ three test examples known as poly-crystalline Photowatt-PWP201 [38], mono-crystalline STM6-40/36 [87], and poly-crystalline STP6-120/36 [87] under a temperature of 45 °C, 51 °C, and 55 °C, respectively. Each of them contains 36 solar cells connected in series. Table 2 presents the lower and upper bounds of each parameter for each PV model, which are widely found in most of the previous studies [39,70,73,77].

Additionally, two commercial models are investigated: mono-crystalline SM55 and thin-film ST40 [34,57] taken from the manufacturer's datasheet to further demonstrate the practicability and reliability of IMPA at different levels of solar irradiation and temperature. Table 3 records the ranges of each parameter for those two models. The variable I_{sc} is determined at non-standard test conditions using the data sheet parameters at STC as follows:

$$I_{sc} = I_{sc-STC} * \frac{G}{G_{STC}} + \propto (T - T_{STC}) \tag{31}$$

where I_{sc-STC} and $\propto$ indicate the short circuit current and the temperature coefficient of the short circuit current. T and G refers to the temperature and the solar irradiance levels at non-standard conditions, while T_{STC} and G_{STC} refers to the temperature and the solar irradiance levels at STC.

5.2. Parameter settings

The parameter tuning of an algorithm can significantly influence the performance of the algorithm. Accordingly, the efficiency of the proposed algorithm has been tested with different values for each parameter. At first, we try various values for the parameter *FADS* (0.1, 0.2, 0.5, 0.7, and 0.9) to study the effect of this parameter on the standard MPA, while the p value is 0.5. Also, we test the following values for$p$: 0.1, 0.5, 1, 1.5, and 2, while *FADS* is 0.2. Several experiments were conducted to select the optimal values for the two parameters by trial and error on different PV models—optimal values of FADS = 0.2 and p = 0.5 were selected as they achieve the best RMSE values in most PV models as concluded from the results presented in Table 4. In this table, we select the DDM as it is more complicated as we need to predict seven parameters. By inspecting the results, we can find that when FADS = 0.2 and p = 0.5, MPA achieves better mean RMSE and Max RMSE values. Although FADS = 0.2 and p = 1.5 obtain the best Min RMSE, The performance of MPA is degraded for the mean RMSE and Max RMSE. Hence, our proposed algorithm uses the following values for the parameters (FADS = 0.2 and p = 0.5). Moreover, the population size was set to 20 as increasing the population size to 30, 40, and 50 did not significantly affect the results (although a lower population size is 10 does produce worse results). The number of evaluations is set to 20,000 for all the next experiments for our proposed algorithm.

The proposed algorithm is compared with other selected existing algorithms:

1. Classified Perturbation Mutation Based Particle Swarm Optimization Algorithm (CPMPSO) (2020) [34].
2. Enhanced Adaptive Differential Evolution (EJADE)) (2020) [35].
3. Improved JAYA (IJAYA) (2017) [39].
4. Memetic Adaptive Differential Evolution (MADE) (2019) [55].
5. Improved Teaching Learning-Based Optimization (ITLBO) (2019) [70].
6. Multiple Learning Backtracking Search Algorithm (MLBSA) (2018) [73].
7. An Improved JADE (Rcr-IJADE) (2013) [77].
8. Whale Optimization Algorithm (WOA) (2018) [88].
9. Success-History based Adaptive Differential Evolution with Linear decrease in population size (L_SHADE) (2014) [89].

For a fair comparison, the parameters of the algorithms are set as suggested by their authors for the best performance of that algorithm. Each algorithm is evaluated 30 times. Table 5 provides the parameters for the proposed IMPA algorithm and the other algorithms.

5.3. The effect of population improvement strategy on IMPA

To further investigate the superiority and the effect of the PIS on the performance of the proposed algorithm, seven test examples representing the different PV models were used, including SDM, DDM, Photowatt-PWP201, STM6-40/36, STP6-120/36, mono-crystalline SM55, and thin-film ST40. Table 6 presents a comparison between the standard MPA (IMPA without PIS) and IMPA in terms of minimum RMSE (Min RMSE), mean RMSE, and maximum RMSE (Max RMSE). The number of iterations is 20,000 and the population size is 20 for the two algorithms to guarantee a fair comparison. We can calculate Min RMSE, mean RMSE, and Max RMSE as follows:

$$MinRMSE = minf_i, i = 1, \cdots, Rn \tag{32}$$

$$MeanRMSE = \frac{1}{Rn} * \sum_{i=1}^{Rn} f_i \tag{33}$$

$$MaxRMSE = maxf_i, i = 1, \cdots, Rn \tag{34}$$

where Rn = 30 is the number of times each algorithm is run. f_i is the

Table 4
The results of MPA using different FADS and p values for DDM.

FADS and p values	Min RMSE	Mean RMSE	Max RMSE
FADS = 0.1, p = 0.5	9.82484851785217E-4	9.829388883641403E-4	9.860218778916113E-4
FADS = 0.2, p = 0.5	9.824848517851832E-4	9.82894433362245E-4	9.860219299974802E-4
FADS = 0.5, p = 0.5	9.824848517852505E-4	9.830496001166087E-4	9.860218778916458E-4
FADS = 0.7, p = 0.5	9.824848517852789E-4	9.830928569377643E-4	9.860218778916852E-4
FADS = 0.9, p = 0.5	9.824904390067673E-4	9.852545755482623E-4	9.927303449610398E-4
FADS = 0.2, p = 0.1	9.824848517852233E-4	9.831289412626381E-4	9.860218779591007E-4
FADS = 0.2, p = 0.5	9.824848517854978E-4	**9.828204393837663E-4**	**9.860218778915734E-4**
FADS = 0.2, p = 1	9.824848517852377E-4	9.830743561369802E-4	9.860218778919765E-4
FADS = 0.2, p = 1.5	**9.824848517851535E-4**	9.829129802869522E-4	9.860218778915838E-4
FADS = 0.2, p = 2	9.824848517852032E-4	9.832127510780706E-4	9.87697877385122E-4

Table 5
Parameter settings for the algorithms.

Algorithm	Parameter	Value
CPMPSO	Population size	50
	Number of function evaluations	50,000
	Acceleration coefficient (c_1)	1.49445
	Acceleration coefficient (c_2)	1.49445
	Inertia weight (w)	0.7298
EJADE	Population size	50
	Number of function evaluations	10,000 for the single diode and Photowatt-PWP201 20,000 for the double diode model 15,000 for STM6-40/36 and STP6-120/36 50,000 for SM55 and ST40
	The largest population size (μ_{max})	50
	The smallest population size (μ_{min})	4
	The crossover rate	The normal distribution in [μ_{CR}, 0.1], μ_{CR}=0.5
MADE	Population size	20
	Number of function evaluations	5000 for the single diode and Photowatt-PWP201 10,000 for the double diode model 7000 for STM6-40/36 and STP6-120/36 50,000 for SM55 and ST40
	The constant value (ε)	0.05 for the single diode and Photowatt-PWP201 0.01 for the double diode model 1.5 for STM6-40/36 and STP6-120/36 0.05 for SM55 and ST40
ITLBO	Population size	50
	Number of function evaluations	50,000
MLBSA	Population size	50
	No. of iterations	50,000
WOA	Population size	50
	Number of function evaluations	50,000
	b	1
IJAYA	Population size	20
	Number of function evaluations	50,000
L_SHADE	Population size	50
	Number of function evaluations	10,000 for the single diode and Photowatt-PWP201 20,000 for the double diode model 30,000 for STM6-40/36 and STP6-120/36 50,000 for SM55 and ST40
Rcr-IJADE	Population size	20
	Number of function evaluations	10,000 for all except for the double diode model is 20,000 50,000 for SM55 and ST40
	The crossover rate (CR)	The normal distribution in [μ_{CR}, 0.1], μ_{CR}=0.5
	The mutation rate (*F*)	Cauchy distribution in [μ_F, 0.1], μ_F=0.5
IMPA	Population size	20
	Number of function evaluations	20,000
	FADs	0.2
	p	0.5
	Mutation probability	0.5

attained fitness at run number *i*. In contrast to*MinRMSE*, which is the minimum RMSE obtained through the thirty runs for each algorithm; Max RMSE is concerned with the maximum RMSE obtained from these runs. RMSE for the mono-crystalline and thin-film ST40 is calculated under STC (1000 W/m^2 and 25 °C). The bold font indicates the best results. By observing the results, we can see that IMPA outperforms standard MPA. The success of IMPA results from the PIS that raises the quality of solutions inside the population based on the mean fitness computed overall for this population.

5.4. The results of IMPA and other existing algorithms

This section concerns about introducing the obtained results by IMPA in comparison with some of the algorithms selected from the literature. In the following subsections, we will investigate the performance of the algorithms using two types of datasets categorized as benchmark data and PV models data from the manufacturer's datasheet

5.4.1. The results of the benchmark data

The subsection contains the results obtained by IMPA, as summarised in Table 7. The parameter estimation of the PV system is a minimization problem that minimizes the RMSE. As mentioned before, DDM is more complicated as there are seven unknown parameters to optimize, while there are five unknown parameters for the other PV models. Table 7 introduces the optimal values of the parameters for each PV model that results in a minimum RMSE in addition to the CPU time in seconds taken by IMPA. With the increase in the number of unknown parameters, the algorithm consumes more time. IMPA achieves a CPU time of 5.88 s. The other test examples take from 3.43 to 3.89 s.

To prove the efficacy of the proposed algorithm, several comparisons were conducted and statistical analyses with other existing algorithms. Furthermore, the choice for these algorithms depends on selecting the most modern and powerful algorithms developed for solving the parameter estimation problem in photovoltaic systems. As discussed in section 5.2 the algorithms are CPMPSO, EJADE, MADE, ITLBO, MLBSA, WOA, IJAYA, L_SHADE, and Rcr-IJADE.

For the SDM, Table 8 lists the performance measures, including Min RMSE, mean RMSE, Max RMSE, and Standard Deviation (SD) values obtained by the different algorithms. The rank (R) is employed to rank the algorithms according to each performance measure. In terms of the Min RMSE, it is evident that IMPA obtains the best RMSE with a value of 9.860218778914944E-4. The remaining algorithms have inferior RMSE

Table 6
Comparison between the standard MPA and IMPA algorithms.

PV model	RMSE	MPA	IMPA
SDM	Min RMSE	9.860218778916844E-4	**9.860218778914944E-4**
	Mean RMSE	9.860218778918169E-4	**9.860218778915467E-4**
	Max RMSE	9.860218778920938E-4	**9.860218778915688E-4**
DDM	Min RMSE	9.824848517854978E-4	**9.824848517852314E-4**
	Mean RMSE	9.828204393837663E-4	**9. 8248485178525E-4**
	Max RMSE	9.860218778915734E-4	**9. 824848517852563E-4**
Photowatt-PWP201	Min RMSE	0.0024250748680951584	**0. 0,024,250,748,680,949,737**
	Mean RMSE	0.002425074868095218	**0. 0,024,250,748,680,950,166**
	Max RMSE	0.0024250748680953718	**0. 002,425,074,868,095,052**
STM6-40/36	Min RMSE	0.0017298137099407108	**0.0017298137099406**
	Mean RMSE	0.0017298137099407424	**0.0017298137099406735**
	Max RMSE	0.0017298137099407828	**0.0017298137099406 82**
STP6-120/36	Min RMSE	0.01660060312508567	**0.01660060312508517**
	Mean RMSE	0.01660060312508619 7	**0.01660060312508531 6**
	Max RMSE	0.01660060312508671 4	**0.01660060312508543 4**
Mono-crystalline SM55	Min RMSE	0.0011462146442649237	**0.0011462146442647702**
	Mean RMSE	0.001146214644265168	**0.0011462146442648227**
	Max RMSE	0.0011462146442655229	**0.0011462146442648574**
Thin-film ST40	Min RMSE	7.34098527340584E-4	**7.340985273403647E-4**
	Mean RMSE	7.340985273408175E-4	**7.340985273404539E-4**
	Max RMSE	7.340985273410204E-4	**7.340985273405078E-4**

Bold values indicate the best results.

Table 7
The obtained estimated values of the parameters for the different PV models by IMPA.

PV model	No. of unknown parameters	Parameter	Estimated value	Min RMSE	CPU time
SDM	1	I_{ph}(A)	0.760775530386165	9.860218778914944E-4	3.89
	2	$I_{sd}(\mu A)$	0.3230208166104389		
	3	$R_s(\Omega)$	0.03637709258093378		
	4	$R_{sh}(\Omega)$	53.71852391990669		
	5	n	1.4811835921250962		
DDM	1	I_{ph}(A)	0. 7,607,810,791,053,599	9. 824848517852314E-4	5.88
	2	$I_{sd1}(\mu A)$	0. 2,259,741,704,682,838		
	3	$I_{sd2}(\mu A)$	0.7493481960748602E		
	4	$R_s(\Omega)$	0. 0,367,404,307,398,601		
	5	$R_{sh}(\Omega)$	55. 48,544,250,733,054		
	6	n_1	1. 4,510,167,292,845,788		
	7	n_2	1. 9,999,999,999,983,524		
Photowatt-PWP201	1	I_{ph}(A)	1. 0,305,142,984,921,734	0. 0,024,250,748,680,949,737	3.81
	2	$I_{sd}(\mu A)$	3. 482,262,904,304,316		
	3	$R_s(\Omega)$	0. 03,336,863,915,936,967		
	4	$R_{sh}(\Omega)$	27. 277,286,205,307,004		
	5	n	1. 3,511,898,569,962,868		
STM6-40/36	1	I_{ph}(A)	1.6639047771123363	0.0017298137099406 6	3.43
	2	$I_{sd}(\mu A)$	1.7386569293847974E-6		
	3	$R_s(\Omega)$	0.004273771168135574		
	4	$R_{sh}(\Omega)$	15.92829416422259		
	5	n	1.520302923702416		
STP6-120/36	1	I_{ph}(A)	7.4725299214116445	0.01660060312508517	3.69
	2	$I_{sd}(\mu A)$	2.334994942900691		
	3	$R_s(\Omega)$	0.004594634622066384		
	4	$R_{sh}(\Omega)$	22.219898772735455		
	5	n	1.2601034740470882		
Mono-crystalline SM55	1	I_{ph}(A)	3.4501035645382037	0.0011462146442647702	3.75
	2	$I_{sd}(\mu A)$	0.17115391913632508		
	3	$R_s(\Omega)$	0.32914770549060207		
	4	$R_{sh}(\Omega)$	483.90046283621217		
	5	n	1.1963595924088781		
Thin-film ST40	1	I_{ph}(A)	2.6757998165992927	7.340985273403647E-4	3.88
	2	$I_{sd}(\mu A)$	1.5288026981486326		
	3	$R_s(\Omega)$	1.1132259839586007		
	4	$R_{sh}(\Omega)$	357.59843785349005		
	5	n	1.5002799446474748		

Table 8
Comparisons on the statistical results of different algorithms for the single diode model.

Algorithm	RMSE							
	Min	R	Mean	R	Max	R	SD	R
CPMPSO	9.8602187789151E-4	2	9.86021877892E-4	4	9.86021877891608E-4	2	2.23388597061E-14	8
EJADE	9.86021877891542E-4	4	9.86021877891636E-4	3	9.86021877891768E-4	5	5.25210013035504E-17	4
MADE	9.86021877893917E-4	8	9.86021878E-4	5	9.86021877903399E-4	8	2.36309962E-15	7
ITLBO	9.86021877891524E-4	3	9.86021877891585E-4	2	9.8602187789162E-4	3	2.29246595256206E-17	2
MLBSA	9.86021877891645E-4	7	9.86021877892E-4	4	9.86021877891985E-4	6	1.01737288291E-16	5
WOA	9.862757377613492E-4	10	0.001035615730260341	7	0.0014095013928157071	10	9.88134343813E-5	10
IJAYA	9.86174762922815E-4	9	9.97834843663E-4	6	0.00103216516431755	9	1.13356387541E-5	9
L_SHADE	9.86021877891594E-4	5	9.86021878E-4	5	9.86021877893691E-4	7	3.9089E-16	6
Rcr-IJADE	9.86021877891609E-4	6	9.86021878E-4	5	9.86021877891745E-4	4	3.643E-17	3
IMPA	**9.860218778914944E-4**	**1**	**9.860218778915467E-4**	**1**	**9.860218778915688E-4**	1	1.7185522162018E-17	**1**

Bold values indicate the best results.

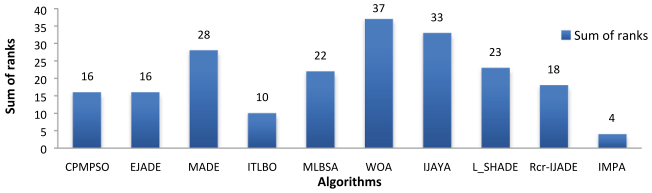

Fig. 6. Comparison of the sum of ranks among algorithms for the SDM.

values, and WOA is the worst with 9.862757377613492E-4. Additionally, for the mean RMSE and Max RMSE, IMPA exhibits a remarkable outperformance, and the standard deviation among the RMSE values is the lowest.

Fig. 6 shows the Sum of Ranks (SR) achieved by each algorithm for all the performance measures. By inspecting the figure, IMPA gets the minimum SR (4), followed by ITLBO (10), EJADE (16), CPMPSO (16), and Rcr-IJADE (18). The SR provides a precise measure as it sums all the ranks for all the performance measures recorded in Table 8.

Although the RMSE values obtained by the algorithms are very close, any decrease in the RMSE may result in a significant identification of the actual parameters of the PV model. Hence, for further recognizing the performance of the proposed algorithm, we use the Individual Absolute Errors (IAE) of the current and the power between the measured and the simulated or the estimated data. $IAE_{current}$ and IAE_{power} are calculated as follows:

$$IAE_{current} = |I_{measured} - I_{estimated}| \tag{35}$$

$$IAE_{power} = (V^{*}I_{measured}) - (V^{*}I_{estimated}) \tag{36}$$

where $I_{estimated}$ denotes the output current estimated using Eq. (5), Eq. (9), or Eq. (10) for the different models. The summation of $IAE_{current}$ is 2.15E-02, which corresponds to 8.730779E-03 of the power, which is such a small amount of power. Table 9 provides the IAE values on the current that illustrates the difference between the measured current and the estimated output current resulting from the estimated parameters obtained by IMPA. The sum of all the IAE values on the current is 2.15E-02 and those in power are small 8.730779E0-3, respectively. Fig. 7 presents a comparison between the measured and estimated data obtained by IMPA to generate the current–voltage (I-V) and the power-voltage (P-V) curves—it can be seen that this estimated data has a high correlation with the measured data over all the voltage data.

Table 9
IAE of IMPA on the single diode model.

Item	The measured data		The estimated current		The estimated power	
	V(V)	$I_{measured}$(A)	$I_{estimated}$(A)	$IAE_{current}$	$P_{estimated}$(W)	IAE_{power}
1	−0.2057	0.7640	0.7640877038354339	8.77038E-05	−0.157172841	1.80407E-05
2	−0.1291	0.7620	0.7626630861797471	0.000663086	−0.098459804	8.56044E-05
3	−0.0588	0.7605	0.761355307150009	0.000855307	−0.044767692	5.02921E-05
4	0.0057	0.7605	0.7601539909944697	0.000346009	0.004332878	1.97225E-06
5	0.0646	0.7600	0.7590552088560624	0.000944791	0.049034966	6.10335E-05
6	0.1185	0.7590	0.7580423451976354	0.000957655	0.089828018	0.000113482
7	0.1678	0.7570	0.7570916539306836	9.16539E-05	0.12703998	1.53795E-05
8	0.2132	0.7570	0.7561413647769484	0.000858635	0.161209339	0.000183061
9	0.2545	0.7555	0.7550868727267279	0.000413127	0.192169609	0.000105141
10	0.2924	0.7540	0.7536638782597733	0.000336122	0.220371318	9.8282E-05
11	0.3269	0.7505	0.7513909665825516	0.000890967	0.245629707	0.000291257
12	0.3585	0.7465	0.747353851511787	0.000853852	0.267926356	0.000306106
13	0.3873	0.7385	0.7401172220871037	0.001617222	0.2866474	0.00062635
14	0.4137	0.7280	0.7273822251610567	0.000617775	0.300918027	0.000255573
15	0.4373	0.7065	0.7069726515095455	0.000472652	0.309159141	0.000206691
16	0.4590	0.6755	0.6752801515576257	0.000219848	0.30995359	0.00010091
17	0.4784	0.6320	0.6307582724300552	0.001241728	0.301754758	0.000594042
18	0.4960	0.5730	0.5719283582846844	0.001071642	0.283676466	0.000531534
19	0.5119	0.4990	0.4996070185873328	0.000607019	0.255748833	0.000310733
20	0.5265	0.4130	0.4136487920563727	0.000648792	0.217786089	0.000341589
21	0.5398	0.3165	0.3175101094076506	0.001010109	0.171391957	0.000545257
22	0.5521	0.2120	0.2121549389330261	0.000154939	0.117130742	8.55418E-05
23	0.5633	0.1035	0.10225131161582138	0.001248688	0.057598164	0.000703386
24	0.5736	−0.0100	−0.00871754177569582	0.001282458	−0.005000382	0.000735618
25	0.5833	−0.1230	−0.12550741271253674	0.002507413	−0.073208474	0.001462574
26	0.5900	−0.2100	−0.20847232628396203	0.001527674	−0.122998673	0.000901327
Sum of IAE				2.15E-02		8.730779E-03

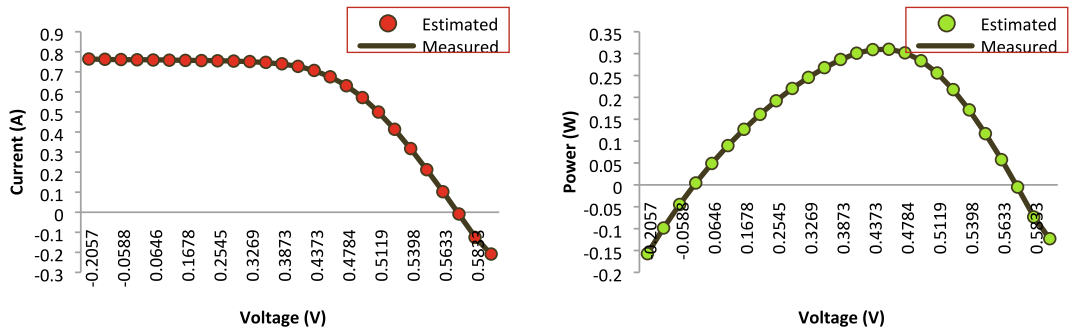

Fig. 7. Comparisons between the experimental data and estimated data obtained by IMPA for SDM: I-V and P-V characteristics.

Table 10
Comparisons on the statistical results of different algorithms for the double diode model.

Algorithm	RMSE							
	Min	R	Mean	R	Max	R	SD	R
CPMPSO	9.82484851785106E-4	**1**	9.83098426093E-4	2	9.86021877891587E-4	3	1.33239583349E-6	3
EJADE	9.82484851872413E-4	5	9.83761445425779E-4	4	9.86031925087449E-4	5	1.45024876914741E-6	4
MADE	9.84821436246726E-4	8	9.86488933E-4	6	9.90514258210889E-4	6	1.64622263E-6	5
ITLBO	9.82485456216039E-4	7	9.9191072606015E-4	7	9.84609324576911E-4	2	1.91123768475037E-6	6
MLBSA	9.82485196598259E-4	6	9.85405654577E-4	5	0.0010010596151342	7	3.45124572331E-6	8
WOA	9.931776928346952E-4	10	9.939390975657772E-4	8	0.0010097208468287243	8	3.00823512934E-6	7
IJAYA	9.8612984637628E-4	9	0.00103285778637	9	0.00136999271943547	9	7.89352619982E-5	9
L_SHADE	9.82484851785345E-4	4	0.00105170971	10	0.00240956742664024	10	2.7701E-4	10
Rcr-IJADE	9.82484851785253E-4	3	9.83379817E-4	3	9.86021877891705E-4	4	1.2827E-6	2
IMPA	9.824848517852314E-4	2	**9.8248485178525E-4**	**1**	**9.824848517852563E-4**	1	7.1359943440015E-18	**1**

Bold values indicate the best results

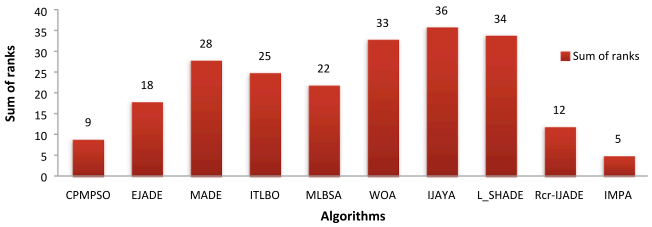

Fig. 8. Comparison of the sum of ranks among algorithms for the DDM.

Table 10 provides a comparison among the algorithms for the DDM. As mentioned above, there are seven parameters to estimate, which makes the optimization process more difficult. By observing the RMSE values, some algorithms show performance degradation like MLBSA, WOA, IJAYA, and L_SHADE. Some algorithms have demonstrated satisfactory performance, such as EJADE, MADE, ITLBO, and Rcr-IJADE. CPMPSO achieves the minimum RSME value, but the proposed algorithm outperforms CPMPSO and the remaining algorithms in terms of mean RMSE and Max RMSE values. Additionally, the variation among the RMSE values is the smallest (7.1359943440015E-18). In Fig. 8, a graphical comparison among the algorithm is presented based on SR. SR gives a complete picture of the order of each algorithm, taking into account the order of that algorithm in all other criteria compared to the other algorithms. IMPA has the lowest SR value (5), as illustrated in the figure. Also, we can find that CPMPSO performs second best with a value of 9, followed by Rcr-IJADE and EJADE.

Table 11 presents the IAE values on the current that expresses the difference between the measured current and the estimated output current resulting from the extracted parameters obtained by IMPA. The sum of all the IAE values on the current and power is 2.13E-02 and 8.776639E0-3, respectively. Fig. 9 shows how the estimated current and power are strictly related to the model curve. IMPA demonstrates high performance for DDM.

For the PV module model, we use three test examples, including Photowatt-PWP201, mono-crystalline STM6-40/36, and poly-crystalline STP6-120/36. There are five parameters to estimate that minimizes the RMSE value. Accordingly, Table 12 reports the experimental results for the Min RMSE, mean RMSE, and Max RMSE. IMPA obtains the best RMSE for all the three test examples compared to the other algorithms. IMPA is ranked first based on the standard deviation among the RMSE values for STM-40/36, while it is second best for Photowtt-PW201 and STP-120/36. As for the remaining algorithms, their performance varies from one test example to another. For instance, EJADE, ITLBO, and CPMPSO are second best for Min RMSE, Mean RMSE, and Max RMSE, respectively, for Photowatt-PWP201. To further provide more insight into the order of the algorithms for the test examples, Figs. 10-12 show the SR for each algorithm. It can be concluded that the proposed algorithm is superior to the rest of the algorithms followed by ITLBO, and WOA is worst for all the test examples.

Tables 13-15 introduce the results of the IAE values on the current and the power to estimate how far the estimated results are from the actual results obtained by the model. For Photowatt-PWP201, all the IAE values on the current are smaller than 0.004833, and the IAE of power is lower than 0.079858135. The sum of IAE on the current is 0.048924, 0.021903, and 0.317128 for Photowatt-PWP201, mono-crystalline STM6-40/36, and poly-crystalline STP6-120/36, and those in power are 0.516888076, 0.284013552, and 4.559227628. The previous comparisons and the statistical analyses ensure the accuracy of the proposed algorithm in extracting the PV parameters. Additionally, Figs. 13-15 depict the I-V and P-V curves for the three test examples to show how the estimated results fit the measured data.

Last but not least, to summarize the performance of the algorithms on the different PV models, Fig. 16 illustrates the order of the algorithms employing the Average Sum of Ranks (ASR). ASR is calculated by the summation of the SR over all the five previous test examples (SDM, DDM, Photowatt-PWP201, STM6-40/36, and STP6-120/36) divided by the number of these test examples (five). In the previous subsections, we

Table 11
IAE of IMPA on the DDM.

Item	The measured data		The estimated current		The estimated power	
	V(V)	$I_{measured}$(A)	$I_{estimated}$(A)	$IAE_{current}$	$P_{estimated}$(W)	IAE_{power}
1	−0.2057	0.7640	0.7639834122428296	1.65878E-05	−0.157151388	3.4121E-06
2	−0.1291	0.7620	0.7626040959280154	0.000604096	−0.098452189	7.79888E-05
3	−0.0588	0.7605	0.7613376981204387	0.000837698	−0.044766657	4.92566E-05
4	0.0057	0.7605	0.7601737876604577	0.000326212	0.004332991	1.85941E-06
5	0.0646	0.7600	0.7591076799214435	0.00089232	0.049038356	5.76439E-05
6	0.1185	0.7590	0.7581214194858976	0.000878581	0.089837388	0.000104112
7	0.1678	0.7570	0.7571886132103789	0.000188613	0.127056249	3.16493E-05
8	0.2132	0.7570	0.7562436063677577	0.000756394	0.161231137	0.000161263
9	0.2545	0.7555	0.7551773009713105	0.000322699	0.192192623	8.21269E-05
10	0.2924	0.7540	0.7537223530462804	0.000277647	0.220388416	8.1184E-05
11	0.3269	0.7505	0.7513991338726065	0.000899134	0.245632377	0.000293927
12	0.3585	0.7465	0.7473014430912753	0.000801443	0.267907567	0.000287317
13	0.3873	0.7385	0.7400106607785395	0.001510661	0.286606129	0.000585079
14	0.4137	0.7280	0.7272469528930021	0.000753047	0.300862064	0.000311536
15	0.4373	0.7065	0.7068502984126499	0.000350298	0.309105635	0.000153185
16	0.4590	0.6755	0.6752105433427432	0.000289457	0.309921639	0.000132861
17	0.4784	0.6320	0.6307607584141811	0.001239242	0.301755947	0.000592853
18	0.4960	0.5730	0.5719947334318536	0.001005267	0.283709388	0.000498612
19	0.5119	0.4990	0.4997061354768926	0.000706135	0.255799571	0.000361471
20	0.5265	0.4130	0.4137336725630098	0.000733673	0.217830779	0.000386279
21	0.5398	0.3165	0.31754620515875676	0.001046205	0.171411442	0.000564742
22	0.5521	0.2120	0.21212299522374725	0.000122995	0.117113106	6.79057E-05
23	0.5633	0.1035	0.10216327581225958	0.001336724	0.057548573	0.000752977
24	0.5736	−0.0100	−0.00879175130192659	0.001208249	−0.005042949	0.000693051
25	0.5833	−0.1230	−0.1255434347039578	0.002543435	−0.073229485	0.001483585
26	0.5900	−0.2100	−0.20837158803142702	0.001628412	−0.122939237	0.000960763
Sum of IAE				2.13E-02		8.776639E0-3

were concerned with the rank of algorithms for each PV model. So, we need an indicator to measure the performance of the algorithms when used with the different PV models. Generally, the ASR provides us with a final order of the algorithms overall the different PV models. From the figure, IMPA surpasses all other algorithms with 4.6, followed by ITLBO, CPMPSO, Rcr-IJADE, EJADE, L_SHADE, MADE, MLBSA, and IJAYA. On the other hand, WOA shows the worst performance. Furthermore, to study the CPU time taken by the algorithms, Fig. 17 shows the average CPU time consumed to run the previous test examples. The average CPU time for each algorithm is calculated as follows:

$$time = \frac{1}{Tn} * \sum_{j=1}^{Tn} AT_j \tag{37}$$

where Tn is the number of the used test examples which is 5. AT_j is the average time taken to run the j^{th} test example. and is computed as:

$$AT = \frac{1}{Rn} * \sum_{i=1}^{Rn} t_i \tag{38}$$

where $Rn = 30$ is the number of times each algorithm is run. t_i determines the time taken by the algorithm at run i for a given test example. Although IMPA doesn't achieve the lowest CPU time, it consumes a reasonable time compared to other algorithms, such as MLBSA, IJAYA, and CPMPSO.

5.4.2. The results of PV models data from the manufacturer's datasheet

In this subsection, the accuracy of the IMPA is tested using two different PV models taken from the manufacturer's datasheet, including thin-film ST40 and mono-crystalline SM55 at various levels of irradiance and temperature. Table 16 reports the estimated results of the five parameters of IMPA for those two PV models. The proposed algorithm estimates the optimal values of the parameters for these two models at different levels of irradiation (200 W/m^2, 400 W/m^2, 600 W/m^2, 800 W/m^2, and 1000 W/m^2), while the temperature is a constant value of 25 °C. For thin-film ST40, we extract the values of the parameters at a temperature of values 25 °C, 40 °C, 55 °C, and 70 °C during G = 1000 W/m^2, and for mono-crystalline SM55, the temperature values are 25 °C, 40 °C, and 60 °C during G = 1000 W/m^2.

Table 17 records the results of the algorithms at different levels of irradiance and a temperature of 25 °C using two performance measures, such as Min RMSE and mean RMSE. According to the Min RMSE, we can

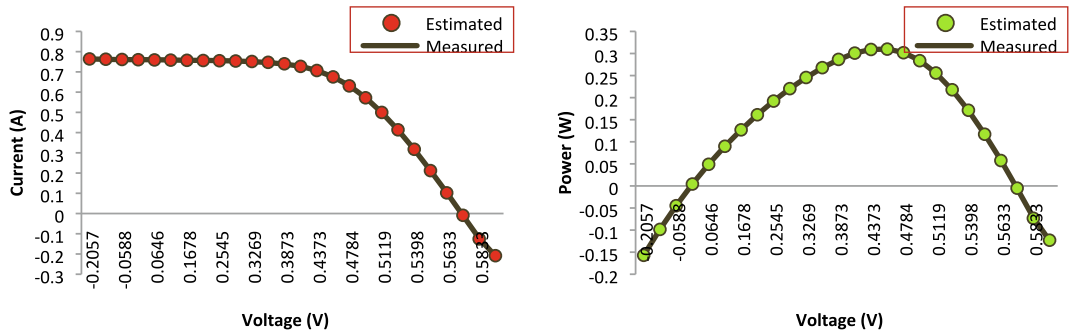

Fig. 9. Comparisons between the experimental data and estimated data obtained by IMPA for DDM: I-V and P-V characteristics.

Table 12
Comparisons on the statistical results of different algorithms on the Photowatt-PWP201 model.

Algorithm	RMSE							
	Min	R	Mean	R	Max	R	SD	R
Photowatt-PWP201								
CPMPSO	0.00242507486809501	4	0.0024250748681	4	0.00242507486809507	2	1.55041302829E-17	3
EJADE	0.00242507486809499	2	0.00242507486809508	3	0.00242507486809514	3	2.82919106054289E-17	4
MADE	0.00242507486809508	8	0.00242507487	5	0.00242507486809525	6	4.13182822E-17	7
ITLBO	0.00242507486809502	5	0.00242507486809505	2	0.00242507486809507	2	1.32971352862898E-17	1
MLBSA	0.002425074868095	3	0.0386685019222	8	0.274250777774058	9	0.0939826232843	10
WOA	0.00260332207066237	10	0.021256249756469923	7	0.04813145342759938	8	0.0223060487855	9
IJAYA	0.00242514540022141	9	0.00243383719844	6	0.00247366726929081	7	0.0000106615319615	8
L_SHADE	0.00242507486809504	7	0.00242507487	5	0.00242507486809516	4	2.9703e-17	5
Rcr-IJADE	0.00242507486809503	6	0.0024250748681	4	0.00242507486809519	5	3.38969193E-17	6
IMPA	0.0024250748680949737	1	0.0024250748680950166	1	0.002425074868095052	1	1.5309200860683E-17	2
STM6-40/36								
CPMPSO	0.00173340318177222	5	0.00173340318177	5	0.00173340318177225	6	7.59208518645E-18	3
EJADE	0.00172981370994069	3	0.0017298137099407	2	0.00172981370994072	4	7.90019463231E-18	4
MADE	0.00172981371001553	4	0.00172981371	4	0.00172981371033432	5	7.48740615E-14	7
ITLBO	0.00172981370994067	2	0.00172981370994068	3	0.0017298137099407	2	6.39942199039336E-18	2
MLBSA	0.00173340318177226	6	0.00173340344936	6	0.001733408271501	7	1.05630408609E-09	8
WOA	0.00359612440522560 96	10	0.0033393845635300364	8	0.0033285220566690718	9	4.86694180592E-5	9
IJAYA	0.00174143178394147	7	0.00192872821646	7	0.00243214397813443	8	0.000180400402203	10
L_SHADE	**0.00172981370994066**	**1**	0.00172981371	4	0.0017298137099407	2	9.744E-18	5
Rcr-IJADE	**0.00172981370994066**	**1**	0.00172981371	4	0.00172981370994071	3	3.3184E-17	6
IMPA	**0.00172981370994066**	**1**	**0.0017298137099406735**	**1**	**0.001729813709940682**	1	**3.98086488349E-18**	**1**
STP6-120/36								
CPMPSO	0.0166006031250852	3	0.0166006031251	3	0.0166006031250856	3	9.94437990268E-17	3
EJADE	0.0166390477687089	7	0.0166390477719	**4**	0.0166390477755783	6	1.8860794921E-10	6
MADE	0.0166006031250869	6	0.0167726726615461	5	0.0166163264	5	0.0000478473421	7
ITLBO	0.0166006031250853	4	0.0166006031250855	2	0.0166006031250856	3	**8.12610993549451E-17**	**1**
MLBSA	0.016600603125086	5	0.0190248493925	7	0.0553470997983828	8	0.00924676516742	9
WOA	0.01866657106822082	9	0.16360659616939385	8	0.268618882068128	9	0.0987788550869	10
IJAYA	0.0166622852078733	8	0.0169333731113	6	0.0176019487151399	7	0.000171325998769	8
L_SHADE	0.0166006031250851	2	0.0166006031251	3	0.0166006031250855	2	1.0634E-16	4
Rcr-IJADE	0.0166006031250851	2	0.0166006031251	3	0.0166006031250858	4	1.808E-16	5
IMPA	**0. 01,660,060,312,508,503**	**1**	**0. 016,600,603,125,085,284**	**1**	**0. 016,600,603,125,085,447**	1	9.8441035668609E-17	2

Bold values indicate the best results.

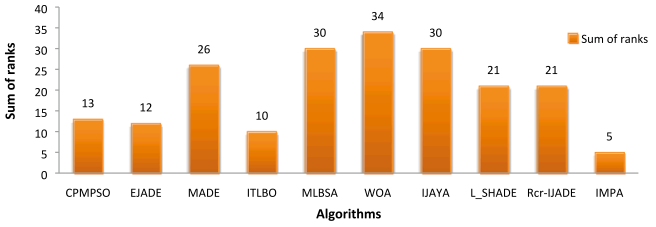

Fig. 10. Comparison of the sum of ranks among algorithms for the Photowatt-PWP201 model.

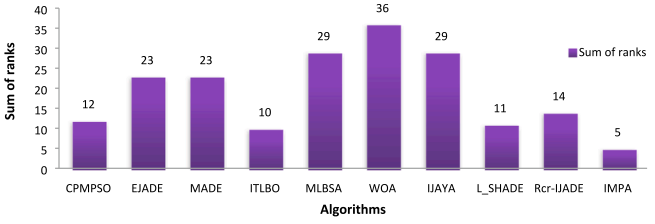

Fig. 12. Comparison of the sum of ranks among algorithms for the STP6-120/36 model.

see that IMPA surpasses the other algorithms in eight out of ten instances, While IMPA wins deservedly in all instances based on mean RMSE. Fig. 18 and Fig. 19 bring a graphical comparison of the I-V characteristics between the measured and estimated data for thin-film ST40 and mono-crystalline SM55, respectively. The figures illustrate the accuracy of IMPA when the irradiance values are varying as the estimated data is in agreement with the measured data. Additionally, the figures in Fig. 20 and Fig. 21 depict the performance of IMPA with varying temperature values for these two models. The results of the estimated output current agree well with the measured current data of the two models.

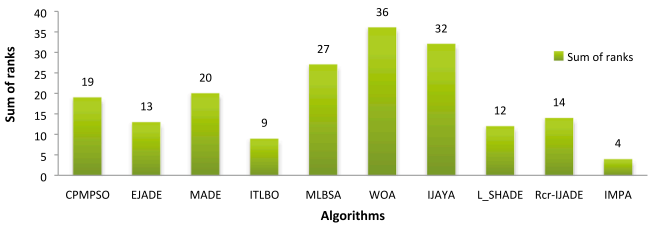

Fig. 11. Comparison of the sum of ranks among algorithms for the STM6-40/36 model.

Through the results of the previous several experiments and the statistical analyses of these results and their comparison with other algorithms, the proposed algorithm outperforms all others in the extraction of optimal parameters for the SDM, DDM, and PV module models and, for practical use, IMPA is shown to be able to estimate the parameters of two different PV models taken from the manufacturer's datasheet. Estimating the efficacy of IMPA depends on several performance metrics, including Min RMSE, mean RMSE, Max RMSE, SD, CPU time, SR, and ASR. IMPA is efficient in terms of time compared to IJAYA, CPMPSO, and MLBSA. Additionally, IMPA outperforms the remaining algorithms in terms of RMSE and SR. The better performance of IMPA results from the good explorative and exploitative capabilities of this algorithm in addition to the utilization of PIS.

Table 13
IAE of IMPA on the Photowatt-PWP201 model.

Item	The measured data		The estimated current		The estimated power	
	V(V)	$I_{measured}$(A)	$I_{estimated}$(A)	$IAE_{current}$	$P_{estimated}$(W)	IAE_{power}
1	0.1248	1.0315	1.0291191612809572	0.002381	0.128434	0.000297129
2	1.8093	1.0300	1.0273810731422448	0.002619	1.858841	0.004738424
3	3.3511	1.0260	1.025741796931723	0.000258	3.437363	0.000865264
4	4.7622	1.0220	1.0241071548175193	0.002107	4.877003	0.010034693
5	6.0538	1.0180	1.0222918046138283	0.004292	6.18875	0.025981727
6	7.2364	1.0155	1.0199306809424948	0.004431	7.380626	0.03206218
7	8.3189	1.0140	1.0163631057488989	0.002363	8.455023	0.01965844
8	9.3097	1.0100	1.0104961513986452	0.000496	9.407416	0.004619021
9	10.2163	1.0035	1.0006289697984485	0.002871	10.22273	0.029331306
10	11.0449	0.9880	0.9845483785599439	0.003452	10.87424	0.038122814
11	11.8018	0.9630	0.9595216761570118	0.003478	11.32408	0.041050482
12	12.4929	0.9255	0.922838818084136	0.002661	11.52893	0.03324588
13	13.1231	0.8725	0.872599662852935	9.97E-05	11.45121	0.001307886
14	13.6983	0.8075	0.8072742637302597	0.000226	11.05829	0.003092203
15	14.2221	0.7265	0.7283364780843768	0.001836	10.35847	0.026118575
16	14.6995	0.6345	0.6371380001439093	0.002638	9.36561	0.038777283
17	15.1346	0.5345	0.5362130633083403	0.001713	8.11537	0.025926528
18	15.5311	0.4275	0.4295113250781632	0.002011	6.670783	0.031238091
19	15.8929	0.3185	0.3187744829421624	0.000274	5.066251	0.00436233
20	16.2229	0.2085	0.20738950680873378	0.00111	3.364459	0.01801542
21	16.5241	0.1010	0.09616717186946928	0.004833	1.589076	0.079858135
22	16.7987	−0.0080	−0.008325386097892296	0.000325	−0.13986	0.005466063
23	17.0499	−0.1110	−0.11093648275911361	6.35E-05	−1.89146	0.001082963
24	17.2793	−0.2090	−0.20924726601505111	0.000247	−3.61565	0.004272584
25	17.4885	−0.3030	−0.300863587104617	0.002136	−5.26165	0.037362657
Sum of IAE				0.048924		0.516888076

6. Managerial implications

This paper presents a promising alternative for the parameter estimation of the PV system to increase its efficiency when producing solar energy. In view of the results of the proposed algorithm, IMPA can accurately predict the values of the PV parameters in comparison with the other existing algorithms for the different PV models in a reasonable time. One great advantage of the proposed algorithm is its ability to reduce the loss of current and power compared to the actual measured current and power of the model. Also, we can see how the figures prove that the estimated data is well fitted to the measured data when changing the temperature and the irradiance values and this is a witness for the efficacy of the IMPA however, the changing environmental conditions. Additionally, for practical use, the performance of IMPA is tested using commercial data extracted from the manufacturer's datasheet, such as thin-film ST40 and mono-crystalline SM55. Therefore, IMPA is an easily implemented and practical approach, as well as a good choice for identifying the optimal parameters of the PV system.

Table 14
IAE of IMPA on the STM6-40/36 module.

Item	The measured data		The estimated current		The estimated power	
	V(V)	$I_{measured}$(A)	$I_{estimated}$(A)	$IAE_{current}$	$P_{estimated}$(W)	IAE_{power}
1	0	1.663	1.6634582557322726	0.000458	0	0
2	0.118	1.663	1.6632523074497643	0.000252	0.196263772	2.97723E-05
3	2.237	1.661	1.6595508062885211	0.001449	3.712415154	0.003241846
4	5.434	1.653	1.653914696871606	0.000915	8.987372463	0.004970463
5	7.26	1.65	1.6505659116709699	0.000566	11.98310852	0.004108519
6	9.68	1.645	1.6454306026241476	0.000431	15.92776823	0.004168233
7	11.59	1.64	1.6392335346800715	0.000766	18.99871667	0.008883333
8	12.6	1.636	1.6337126936519537	0.002287	20.58477994	0.02882006
9	13.377	1.629	1.6272858057215005	0.001714	21.76820222	0.022930777
10	14.09	1.619	1.6183135732852598	0.000686	22.80203825	0.009671752
11	14.88	1.597	1.6030900423814909	0.00609	23.85397983	0.090619831
12	15.59	1.581	1.5815883737423793	0.000588	24.65696275	0.009172747
13	16.4	1.542	1.54233058815657	0.000331	25.29422165	0.005421646
14	16.71	1.524	1.521192630947623	0.002807	25.41912886	0.046911137
15	16.98	1.5	1.49919474141339	0.000805	25.45632671	0.013673291
16	17.13	1.485	1.4852752671836265	0.000275	25.44276533	0.004715327
17	17.32	1.465	1.4656542394637584	0.000654	25.38513143	0.011331428
18	17.91	1.388	1.38758936599565	0.000411	24.85172554	0.007354455
19	19.08	1.118	1.118391374021248	0.000391	21.33890742	0.007467416
20	21.02	0	−2.481062598936462E-5	2.48E-05	−0.000521519	0.000521519
Sum of IAE				0.021903		0.284013552

Table 15
IAE of IMPA on STP6-120/36 model.

Item	The measured data		The estimated current		The estimated power	
	V(V)	$I_{measured}$(A)	$I_{estimated}$(A)	$IAE_{current}$	$P_{estimated}$(W)	IAE_{power}
1	19.21	0	0.0022826028505886324	0.002283	0.043849	0.043848801
2	17.65	3.83	3.833347195618671	0.003347	67.65858	0.059078003
3	17.41	4.29	4.267337583012318	0.022662	74.29435	0.39455268
4	17.25	4.56	4.541148547107021	0.018851	78.33481	0.325187562
5	17.1	4.79	4.784400213277089	0.0056	81.81324	0.095756353
6	16.9	5.07	5.085578070019134	0.015578	85.94627	0.263269383
7	16.76	5.27	5.274822462319878	0.004822	88.40602	0.080824468
8	16.34	5.75	5.782597479690904	0.032597	94.48764	0.532642818
9	16.08	6	6.0443179806667295	0.044318	97.19263	0.712633129
10	15.71	6.36	6.347120906977644	0.012879	99.71327	0.202330551
11	15.39	6.58	6.5665499100330855	0.01345	101.0592	0.206996885
12	14.93	6.83	6.813611048726439	0.016389	101.7272	0.244687043
13	14.58	6.97	6.957709716727478	0.01229	101.4434	0.17919233
14	14.17	7.1	7.087575795025513	0.012424	100.4309	0.176050984
15	13.59	7.23	7.217384864896084	0.012615	98.08426	0.171439686
16	13.16	7.29	7.283999575252194	0.006	95.85743	0.07896559
17	12.74	7.34	7.331345487456747	0.008655	93.40134	0.11025849
18	12.36	7.37	7.363183210220859	0.006817	91.00894	0.084255522
19	11.81	7.38	7.395999854054966	0.016	87.34676	0.188958276
20	11.17	7.41	7.420315759300003	0.010316	82.88493	0.115227031
21	10.32	7.44	7.439089820180148	0.00091	76.77141	0.009393056
22	9.74	7.42	7.446762103664929	0.026762	72.53146	0.26066289
23	9.06	7.45	7.452540407993373	0.00254	67.52002	0.023016096
24	0	7.48	7.470979413229995	0.009021	0	0
Sum of IAE				0.317128		4.559227628

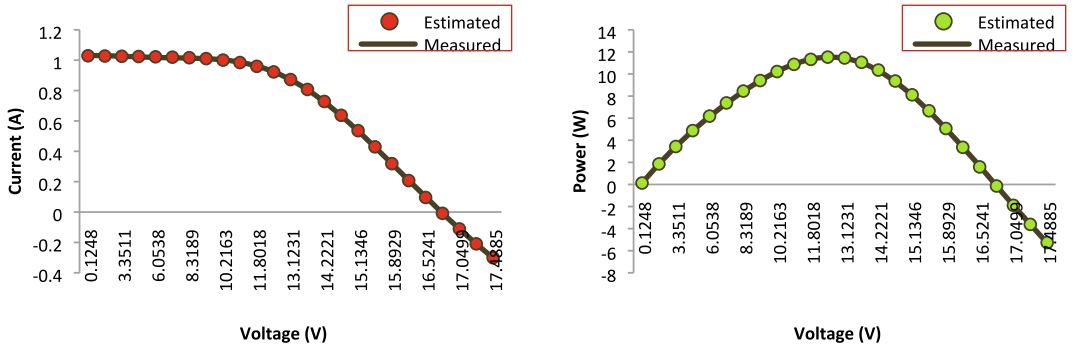

Fig. 13. Comparisons between the experimental data and estimated data obtained by IMPA for Photowatt-PWP201: I-V and P-V characteristics.

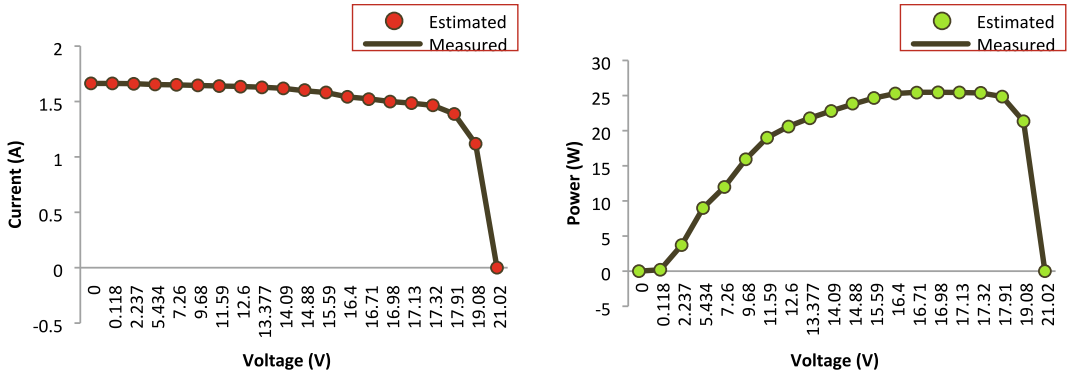

Fig. 14. Comparisons between the experimental data and estimated data obtained by IMPA for STM6-40/36 module: I-V and P-V characteristics.

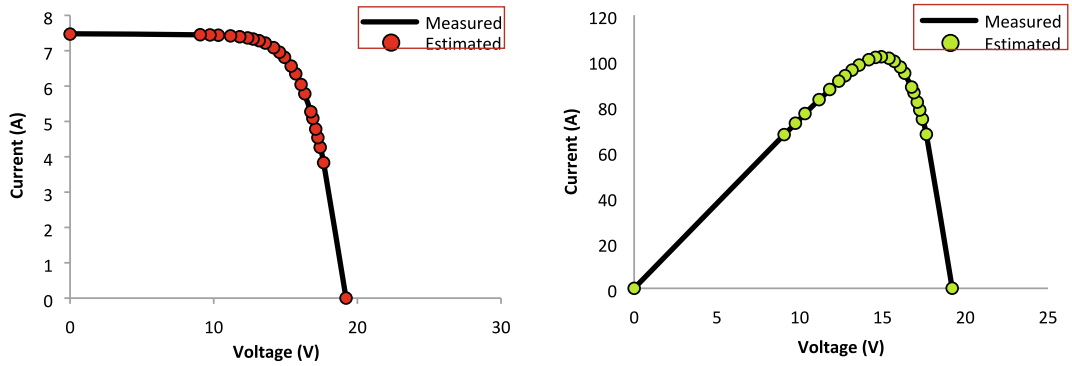

Fig. 15. Comparisons between the experimental data and estimated data obtained by IMPA for STP6-120/36 module: I-V and P-V characteristics.

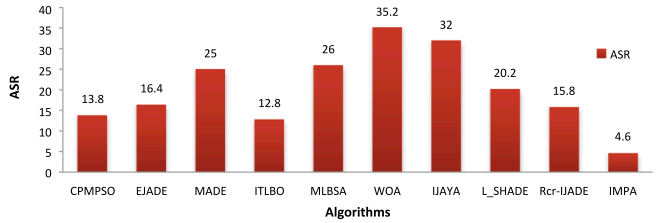

Fig. 16. Comparison of the average sum of ranks among algorithms for the different PV models.

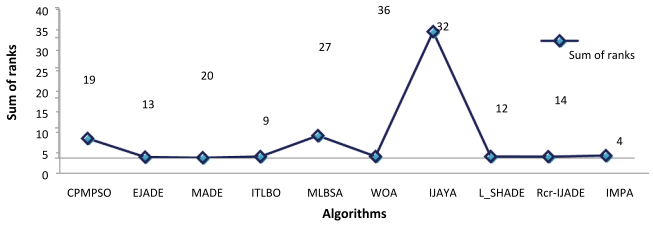

Fig. 17. Average CPU time for running all the different PV models.

7. Conclusions and future work

Parameters estimation is a challenging task in PV systems to optimize the accuracy of the generated current and power. This paper proposes an improved version of the marine predators algorithm for accurately estimating the optimal parameters of the different PV models (SDM, DDM, PV module). For further enhancement of the quality of the solutions, a population improvement strategy is utilized, which splits the solutions inside the population into two categories (high-quality solutions and low-quality solutions). Each category is treated differently based on the mean fitness of the population. For the high-quality solutions, their fitness values are lower than the mean fitness and are handled as a minimization problem and these solutions are updated using an adaptive mutation operation with a probability of 0.5. For the low-quality solutions, the solutions are updated based on the location of the top predator and a good-quality predator selected from the first half of the population after sorting the solutions according to their fitness. To investigate the efficacy of IMPA, several experiments were conducted to make comparisons with the other existing algorithms. The results and the statistical analyses show the superior performance of IMPA in terms of RMSE, SD, CPU time, IAE, SR, and ASR for all the different PV models. Further, the graphical representation of the I-V and P-V characteristics proves that the estimated data agree well with the measured data. Moreover, the efficacy of the IMPA was tested using datasets from the manufacturer's datasheet at different levels of irradiance and temperature and IMPA can be a promising alternative for the parameter estimation of PV systems. Unfortunately, IMPA doesn't achieve the lowest CPU time, so, we need to search for more strategies to reduce the time consumed. Although many PV models have been developed and modified (new one-diode model [25], improved two-diode model [26], modified double-diode model [27], simplified two-diode model [28], and Three-Diode Model (TDM) [29]), IMPA is only tested using three of those types of models.

In the future, the proposed algorithm is planned to be applied to other fields of energy such as maximum power point tracking (MPPT) [90], and the energy scheduling [91] problem of PV systems. A future priority is also in the development of more promising strategies for the proposed algorithm to be able to solve many other optimization problems, especially for constrained and multi-objective problems.

Funding

This research has no funding source.

Ethical approval

This article does not contain any studies with human participants or animals performed by any of the authors.

CRediT authorship contribution statement

Mohamed Abdel-Basset: Investigation, Methodology, Resources, Visualization, Software, Writing - original draft. **Doaa El-Shahat:** Investigation, Methodology, Resources, Visualization, Software, Writing - original draft. **Ripon K. Chakrabortty:** Conceptualization, Methodology. **Michael Ryan:** Investigation, Validation, Supervision.

Declaration of Competing Interest

The authors declare that they have no known competing financial interests or personal relationships that could have appeared to influence the work reported in this paper.

Table 16
The estimated parameters by IMPA at different irradiance and temperature values.

Parameter	Thin-film ST40	Mono-crystalline SM55	Parameter	Thin-film ST40	Mono-crystalline SM55
G = 1000 W/m^2 and T = 25 °C			**T = 40 °C and G = 1000 W/m^2**		
I_{ph}(A)	2.6757998165992927	3.450103564278689	I_{ph}(A)	2.680911955758242	3.4691375162567644
$I_{sd}(\mu A)$	1.5288026981486326	0.17115391729608885	$I_{sd}(\mu A)$	5.666096130223684	1.1451097577028376
$R_s(\Omega)$	1.1132259839586007	0.3291477055271942	$R_s(\Omega)$	1.1292977088674643	0.31309593289804194
$R_{sh}(\Omega)$	357.59843785349005	483.9004717331982	$R_{sh}(\Omega)$	364.1097500409742	533.0691724097478
n	1.5002799446474748	1.1963595916103462	n	1.4764779873804783	1.2152912211326379
RMSE	0.0007340985273403647	0.0011462146442647084	RMSE	0.0013214137338305777	0.003788814654597816
G = 800 W/m^2 and T = 25 °C			**T = 55 °C and G = 1000 W/m^2**		
I_{ph}(A)	2.138014756755787	2.760381699475463	I_{ph}(A)	2.6919684871516676	
$I_{sd}(\mu A)$	1.1581025299414163	0.14395059013877548	$I_{sd}(\mu A)$	1.8680728957581096	
$R_s(\Omega)$	1.125286813191816	0.33759023050729814	$R_s(\Omega)$	1.1495892294050953	–
$R_{sh}(\Omega)$	332.88893580510694	459.8784944179679	$R_{sh}(\Omega)$	295.0217667915861	
n	1.4731489051564084	1.1838381554551365	n	1.519221141793006	
RMSE	0.0007739052137450907	0.0006685794662080992	RMSE	0.001823260065698566	
G = 600 W/m^2 and T = 25 °C			**T = 60 °C and G = 1000 W/m^2**		
I_{ph}(A)	1.6048097229166918	2.0708965439825042	I_{ph}(A)		3.49460846962827
$I_{sd}(\mu A)$	1.4418696976349096	0.15551374081695722	$I_{sd}(\mu A)$		6.909499265024281
$R_s(\Omega)$	1.1126137396794458	0.33050251086425486	$R_s(\Omega)$	–	0.3187057326811052
$R_{sh}(\Omega)$	347.6946832799241	450.0685288716869	$R_{sh}(\Omega)$		484.8839212165347
n	1.495820573864127	1.189315054552899	n		1.204407205586651
RMSE	0.0006740357441638704	0.0008239494020977826	RMSE		0.0037803880658908075
G = 400 W/m^2 and T = 25 °C			**T = 70 °C and G = 1000 W/m^2**		
I_{ph}(A)	1.0675442271845799	1.3828441328023766	I_{ph}(A)	2.6923294766827737	
$I_{sd}(\mu A)$	1.8487469765508373	0.10041951474096452	$I_{sd}(\mu A)$	8.752185380111636	
$R_s(\Omega)$	1.080580312721794	0.3966541223781731	$R_s(\Omega)$	1.125888708589428	
$R_{sh}(\Omega)$	362.5144991466386	427.05044033470887	$R_{sh}(\Omega)$	367.7532338806409	–
n	1.5244544986299657	1.1588470135094666	n	1.4805598883286137	
RMSE	0.0006307245716932746	0.0007076081827351263	RMSE	7.777180424711708E-4	
G = 200 W/m^2 and T = 25 °C					
I_{ph}(A)	0.533137404085902	0.6915098345702557			
$I_{sd}(\mu A)$	1.4296748417356646	1.4641170853620463			
$R_s(\Omega)$	1.1857211713785092	0.2866199515097498			
$R_{sh}(\Omega)$	344.9832436310418	448.21070944790597			
n	1.4975214704035362	1.1834232721135407			
RMSE	0.00047720079229727623	0.0003206875103215443			

Table 17
The results of the algorithms at different irradiance and temperature of 25 °C.

Algorithm	Thin-film ST40		Mono-crystalline SM55	
	Min RMSE	Mean RMSE	Min RMSE	Mean RMSE
G = 1000 W/m^2				
CPMPSO	0.000734098527340430	0.00073409852734053	0.00114621464426481	0.0011462146442649
EJADE	**0.000734098527340347**	0.000734098527340494	0.00114621464426479	0.00114621464426486
MADE	0.000734098527341893	0.00073409852734296	0.00114621464426535	0.0011462146442658
ITLBO	0.00073409852734044	0.000734098527340523	0.00114621464426483	0.00114621464426489
MLBSA	0.000734098527341072	0.00073435964134103	0.00114621464426529	0.0011725790246127
WOA	0.000741519880124711 3	0.00276297867041563 33	0.00116723410456779 76	0.012876187813728616
L_SHADE	0.000734098527340363	0.00073409852734047	0.00114621464426471	0.0013758083166385
Rcr-IJADE	0.000734098527340402	0.00073409852734054	0.0011462146442648	0.0011462146442649
IMPA	0.000734098527340 3647	**0.000734098527340 4539**	**0.001146214644264 7084**	**0. 0,011,462,146,442,647,889**
G = 800 W/m^2				
CPMPSO	0.000773905213745151	0.00077390521374522	0.000668579466208175	0.00066857946620825
EJADE	0.000773905213745109	0.000773905213745208	0.000668579466208092	0.000668579466208246
MADE	0.000773905213746688	0.00077390521374807	0.000668579466208794	0.00066857946620977
ITLBO	0.000773905213745162	0.000773905213745224	0.000668579466208222	0.000668579466208269
MLBSA	0.000773905213745336	0.00077392053012588	0.000668579466208516	0.00066947380384539
WOA	0.000775234556628146	0.00188174408995652 84	0.00067359932316370 35	0.0017152947717123965
L_SHADE	0.000773905213745118	0.00077390521374518	0.000668579466208120	0.00076412343655151
Rcr-IJADE	0.000773905213745111	0.00077390521374522	0.000668579466208143	0.00066857946620826
IMPA	**0.000773905213745090 7**	**0.000773905213745161**	**0.000668579466208099 2**	**0.000668579466208166 5**
G = 600 W/m^2				
CPMPSO	0.000674035744163936	0.00067403574416396	0.000823949402097821	0.00082394940209786
EJADE	0.000674035744163 9	0.000674035744163949	0.00082394940209776	0.00082394940209785
MADE	0.000674035744164875	0.00067403574416613	0.000823949402098443	0.00082394940209906
ITLBO	0.000674035744163922	0.00067403574416396	0.000823949402097836	0.000823949402097875
MLBSA	0.000674035744164005	0.00067403577483217	0.000823949402098047	0.00082395136296965
WOA	0.000676127947161 0844	0.00149705673318956 01	0.00082559363543295 2	0.0018663841387298184
L_SHADE	0.000674035744163877	0.00067403574416393	**0.000823949402097732**	0.00082394940209783
Rcr-IJADE	0.000674035744163905	0.00067403574416396	0.000823949402097801	0.00082394940209788
IMPA	**0.000674035744163 8704**	**0.000674035744163915**	0.000823949402097826	**0.000823949402097 8095**
G = 400 W/m^2				
CPMPSO	0.000630724571693316	0.00063072457169334	0.000707608182735 1490	0.00070760818273516
EJADE	0.000630724571693301	0.000630724571693338	0.00070760818273514 4	0.000707608182735167
MADE	0.000630724571693984	0.00063072457169573	0.00070760818273562 3	0.00070760818273663
ITLBO	0.000630724571693326	0.000630724571693352	0.00070760818273515 3	0.000707608182735167
MLBSA	0.000630724571693361	0.00063072457221925	0.00070760818273518 0	0.00070760845971413
WOA	0.000630905270463332 8	0.00102975342873179 94	0.00078101548437880 42	0.0022949332084046038
L_SHADE	0.000630724571693276	0.00063072457169331	0.00070760818273513 7	0.00091712850061672
Rcr-IJADE	0.000630724571693278	0.00063072457169334	0.00070760818273515 0	0.00070760818273517
IMPA	**0.000630724571693 2746**	**0.000630724571693 3049**	**0.000707608182735 1263**	**0.000707608182735 1496**
G = 200 W/m^2				
CPMPSO	0.000477200792297284	0.0004772007922973	0.000320687510321552	0.00032068751032156
EJADE	0.000477200792297281	0.000439699477753208	0.000320687510321549	0.000320687510321563
MADE	0.000477200792298183	0.00047720079230084	0.000320687510322113	0.00032068751032362
ITLBO	0.000477200792297291	0.000477200792297297	0.000320687510321553	0.000320687510321561
MLBSA	0.000477200792297310	0.00047993828215249	0.000320687510321567	0.00032068751033118
WOA	0.000477511087011580 47	0.00052132422864034 18	0.00062058301867508 57	0.00062065122985349
L_SHADE	0.000477200792297280	0.00047720079229729	0.000320687510321547	0.00032068751032156
Rcr-IJADE	0.000477200792297282	0.0004772007922973	0.000320687510321554	0.00032068751032156
IMPA	**0.000477200792297 27623**	**0.000477200792297 2862**	**0.000320687510321 5443**	**0.000320687510321 55466**

Bold values indicate the best results.

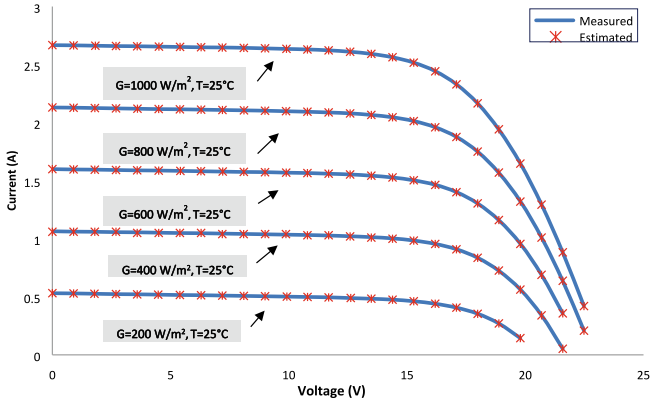

Fig. 18. Comparisons between experimental and estimated data for the thin-film ST40 module at different irradiance values.

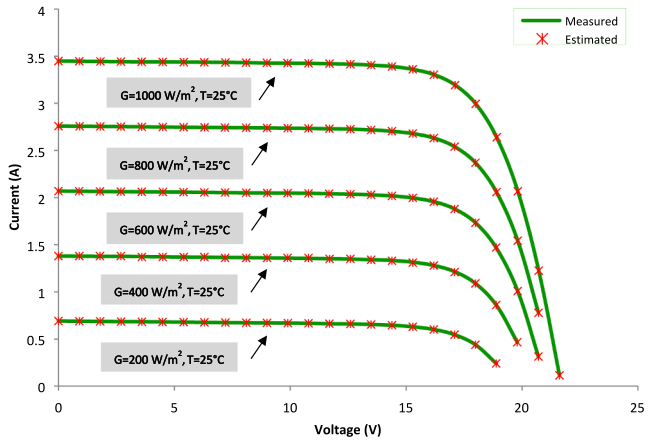

Fig. 19. Comparisons between measured and estimated data for the mono-crystalline SM55 module at different irradiance values.

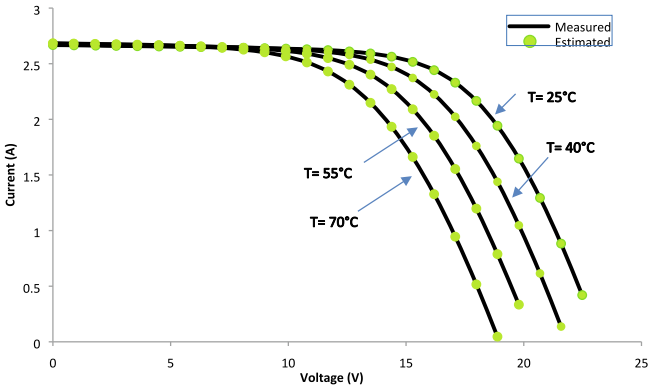

Fig. 20. Comparisons between measured and estimated data for the thin-film ST40 module at different temperature values.

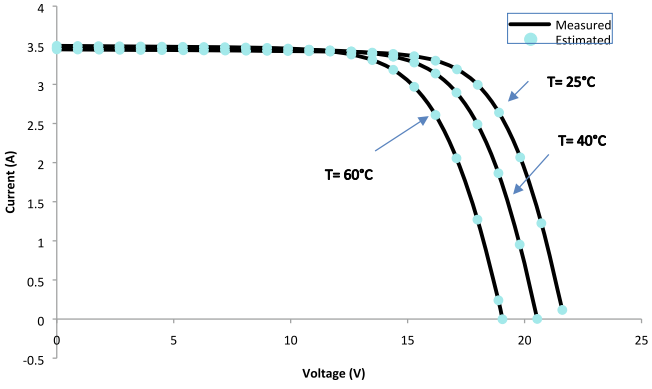

Fig. 21. Comparisons between measured and estimated data for the mono-crystalline SM55 module at different temperature values.

References

[1] Perera. F. Pollution from fossil-fuel combustion is the leading environmental threat to global pediatric health and equity: Solutions exist. International journal of environmental research and public health. 15; 2018: 16.

[2] Qais MH, Hasanien HM, Alghuwainem S, Nouh AS. Coyote optimization algorithm for parameters extraction of three-diode photovoltaic models of photovoltaic modules. Energy 2019;187:116001.

[3] Li H, Sun Y. Operational performance study on a photovoltaic loop heat pipe/solar assisted heat pump water heating system. Energy Build 2018;158:861–72.

[4] Shafieian A, Osman JJ, Khiadani M, Nosrati A. Enhancing heat pipe solar water heating systems performance using a novel variable mass flow rate technique and different solar working fluids. Sol Energy 2019;186:191–203.

[5] Sutopo W, Mardikaningsih IS, Zakaria R, Ali A. A Model to Improve the Implementation Standards of Street Lighting Based on Solar Energy: A Case Study. Energies 2020;13:630.

[6] Mulyana, E. Setiawan, A.E. Sumaryo, S. Munir. A. Data Monitoring System of Solar Module with Data Logger for Public Street Lighting Application. 2019 26th International Conference on Telecommunications (ICT). IEEE; 2019. pp. 280-3.

[7] Pang W, Yu H, Zhang Y, Yan H. Solar photovoltaic based air cooling system for vehicles. Renewable Energy 2019;130:25–31.

[8] Mehrjerdi H, Rakhshani E. Vehicle-to-grid technology for cost reduction and uncertainty management integrated with solar power. J Cleaner Prod 2019;229: 463–9.

[9] Odabaşı V, Maglio S, Martini A, Sorrentino S. Static stress analysis of suspension systems for a solar-powered car. FME Transactions. 2019;47:70–5.

[10] Santra P, Pande P, Kumar S, Mishra D, Singh R. Agri-voltaics or Solar farming: the concept of integrating solar PV based electricity generation and crop production in a single land use system. Int J Renew Energy Res (IJRER). 2017;7:694–9.

[11] Michalena E, Tripanagnostopoulos Y. Contribution of the solar energy in the sustainable tourism development of the Mediterranean islands. Renewable Energy 2010;35:667–73.

[12] Barman A, Neogi B, Pal S. Solar-Powered Automated IoT-Based Drip Irrigation System. IoT and Analytics for Agriculture. Springer 2020:27–49.

[13] Ghosal M, Sahoo N, Goel S. Studies on Off-Grid Solar Photovoltaic-Powered Micro-Irrigation System in Aerobic Rice Cultivation for Sustainable Agriculture and Mitigating Greenhouse Gas Emission. Innovation in Electrical Power Engineering, Communication, and Computing Technology. Springer 2020:135–45.

[14] Da Silva I, Ronoh G, Maranga I, Odhiambo M, Kiyegga R. Implementing the SDG 2, 6 and 7 Nexus in Kenya—A Case Study of Solar Powered Water Pumping for Human Consumption and Irrigation. International Business, Trade and Institutional Sustainability. Springer 2020:933–42.

[15] Bayod-Rújula AA. In: Solar Hydrogen Production. Elsevier; 2019. p. 237–95. https://doi.org/10.1016/B978-0-12-814853-2.00008-4.

[16] Congedo P, Malvoni M, Mele M, De Giorgi M. Performance measurements of monocrystalline silicon PV modules in South-eastern Italy. Energy Convers Manage 2013;68:1–10.

[17] Mattei M, Notton G, Cristofari C, Muselli M, Poggi P. Calculation of the polycrystalline PV module temperature using a simple method of energy balance. Renewable Energy 2006;31:553–67.

[18] Qarony W, Hossain MI, Hossain MK, Uddin MJ, Haque A, Saad A, et al. Efficient amorphous silicon solar cells: characterization, optimization, and optical loss analysis. Results Phys 2017;7:4287–93.

[19] Snyder GH, Matichenkov VV, Datnoff LE. Silicon. Handbook of plant nutrition. CRC Press; 2016. p. 567–84.

[20] Singh R. Why silicon is and will remain the dominant photovoltaic material. J. Nanophoton 2009;3(1):032503. https://doi.org/10.1117/1.3196882.

[21] Patlins, A., Hnatov, A. Arhun, S. Hnatova, H. Migal. V. Study of load characteristics of various types of silicon PV panels for sustainable energy efficient road pavement. Electrical, control and communication engineering. 15 (2019) 30-8.

[22] Geissler J, Helmreich D. Process for the manufacture of coarsely crystalline to monocrystalline sheets of semiconductor material. Google Patents 1984.

[23] Makrides G, Zinsser B, Norton M, E. G. In: Third Generation Photovoltaics. InTech; 2012. https://doi.org/10.5772/27386.

[24] Schropp RE, Zeman M. New developments in amorphous thin-film silicon solar cells. IEEE Trans Electron Devices 1999;46:2086–92.

[25] Orioli A. An accurate one-diode model suited to represent the current-voltage characteristics of crystalline and thin-film photovoltaic modules. Renewable Energy 2020;145:725–43.

[26] Salam, Z. Ishaque, K. Taheri. H. An improved two-diode photovoltaic (PV) model for PV system. 2010 Joint International Conference on Power Electronics, Drives and Energy Systems & 2010 Power India. IEEE; 2010. pp. 1-5.

[27] Bühler AJ, Krenzinger A. Method for photovoltaic parameter extraction according to a modified double-diode model. Prog Photovoltaics Res Appl 2013;21:884–93.

[28] Babu BC, Gurjar S. A novel simplified two-diode model of photovoltaic (PV) module. IEEE J Photovoltaics 2014;4:1156–61.

[29] Khanna V, Das B, Bisht D, Singh P. A three diode model for industrial solar cells and estimation of solar cell parameters using PSO algorithm. Renewable Energy 2015;78:105–13.

[30] Wolf P, Benda V. Identification of PV solar cells and modules parameters by combining statistical and analytical methods. Sol Energy 2013;93:151–7.

[31] Batzelis EI, Papathanassiou SA. A method for the analytical extraction of the single-diode PV model parameters. IEEE Trans Sustainable Energy 2015;7:504–12.

[32] Xiao H, Xie S. Leakage current analytical model and application in single-phase transformerless photovoltaic grid-connected inverter. IEEE Trans Electromagn Compat 2010;52:902–13.

[33] Ibrahim H, Anani N. Evaluation of analytical methods for parameter extraction of PV modules. Energy Procedia 2017;134:69–78.

[34] Liang J, Ge S, Qu B, Yu K, Liu F, Yang H, et al. Classified perturbation mutation based particle swarm optimization algorithm for parameters extraction of photovoltaic models. Energy Convers Manage 2020;203:112138.

[35] Li S, Gu Q, Gong W, Ning B. An enhanced adaptive differential evolution algorithm for parameter extraction of photovoltaic models. Energy Convers Manage 2020; 205:112443.

[36] Ortiz-Conde A, Sánchez FJG, Muci J. New method to extract the model parameters of solar cells from the explicit analytic solutions of their illuminated I-V characteristics. Sol Energy Mater Sol Cells 2006;90:352–61.

[37] Tong, N.T. Kamolpattana, K. Pora. W. A deterministic method for searching the maximum power point of a PV panel. 2015 12th International Conference on Electrical Engineering/Electronics, Computer, Telecommunications and Information Technology (ECTI-CON). IEEE; 2015. pp. 1-6.

[38] Easwarakhanthan T, Bottin J, Bouhouch I, Boutrit C. Nonlinear minimization algorithm for determining the solar cell parameters with microcomputers. Int J Solar Energy 1986;4:1–12.

[39] Yu K, Liang J, Qu B, Chen X, Wang H. Parameters identification of photovoltaic models using an improved JAYA optimization algorithm. Energy Convers Manage 2017;150:742–53.

[40] Zhu Z, Zhou X. An efficient evolutionary grey wolf optimizer for multi-objective flexible job shop scheduling problem with hierarchical job precedence constraints. Comput Ind Eng 2020;140:106280. https://doi.org/10.1016/j.cie.2020.106280.

[41] Dhiman G. MOSHEPO: a hybrid multi-objective approach to solve economic load dispatch and micro grid problems. Appl Intellig 2020;50:119–37.

[42] Pham Q-V, Mirjalili S, Kumar N, Alazab M, Hwang W-J. Whale Optimization Algorithm With Applications to Resource Allocation in Wireless Networks. IEEE Trans Veh Technol 2020;69(4):4285–97.

[43] Monal P, Heistrene L, Pandya V. Optimal Power Flow in Power Networks with TCSC Using Particle Swarm Optimization Technique. In: Advances in Electric Power and Energy Infrastructure. Springer; 2020. p. 91–101.

[44] Wang L, Zheng X-L, Wang S-Y. A novel binary fruit fly optimization algorithm for solving the multidimensional knapsack problem. Knowl-Based Syst 2013;48:17–23.

[45] Mafarja MM, Mirjalili S. Hybrid whale optimization algorithm with simulated annealing for feature selection. Neurocomputing. 2017;260:302–12.

[46] Yang B, Wang J, Zhang X, Yu T, Yao W, Shu H, et al. Comprehensive overview of meta-heuristic algorithm applications on PV cell parameter identification. Energy Convers Manage 2020;208:112595.

[47] Qais MH, Hasanien HM, Alghuwainem S. Identification of electrical parameters for three-diode photovoltaic model using analytical and sunflower optimization algorithm. Appl Energy 2019;250:109–17.

[48] Ben Messaoud R. Extraction of uncertain parameters of double-diode model of a photovoltaic panel using Ant Lion Optimization. SN Appl Sci 2020;2(2). https://doi.org/10.1007/s42452-020-2013-z.

[49] Alam D, Yousri D, Eteiba M. Flower pollination algorithm based solar PV parameter estimation. Energy Convers Manage 2015;101:410–22.

[50] Rajasekar N, Kumar NK, Venugopalan R. Bacterial foraging algorithm based solar PV parameter estimation. Sol Energy 2013;97:255–65.

[51] Chen X, Xu B, Mei C, Ding Y, Li K. Teaching–learning–based artificial bee colony for solar photovoltaic parameter estimation. Appl Energy 2018;212:1578–88.

[52] Ishaque K, Salam Z. An improved modeling method to determine the model parameters of photovoltaic (PV) modules using differential evolution (DE). Sol Energy 2011;85:2349–59.

[53] Ishaque K, Salam Z, Mekhilef S, Shamsudin A. Parameter extraction of solar photovoltaic modules using penalty-based differential evolution. Appl Energy 2012;99:297–308.

[54] Biswas PP, Suganthan PN, Wu G, Amaratunga GA. Parameter estimation of solar cells using datasheet information with the application of an adaptive differential evolution algorithm. Renewable Energy 2019;132:425–38.

[55] Li S, Gong W, Yan X, Hu C, Bai D, Wang L. Parameter estimation of photovoltaic models with memetic adaptive differential evolution. Sol Energy 2019;190:465–74.

[56] Rezaee Jordehi A. Enhanced leader particle swarm optimisation (ELPSO): An efficient algorithm for parameter estimation of photovoltaic (PV) cells and modules. Sol Energy 2018;159:78–87.

[57] Merchaoui M, Sakly A, Mimouni MF. Particle swarm optimisation with adaptive mutation strategy for photovoltaic solar cell/module parameter extraction. Energy Convers Manage 2018;175:151–63.

[58] Chen H, Jiao S, Heidari AA, Wang M, Chen X, Zhao X. An opposition-based sine cosine approach with local search for parameter estimation of photovoltaic models. Energy Convers Manage 2019;195:927–42.

[59] Fathy A, Elaziz MA, Sayed ET, Olabi A, Rezk H. Optimal parameter identification of triple-junction photovoltaic panel based on enhanced moth search algorithm. Energy. 2019;188:116025.

[60] Ma J, Ting T, Man KL, Zhang N, Guan S-U, Wong PW. Parameter estimation of photovoltaic models via cuckoo search. J Appl Math 2013;2013:362619.

[61] Kang T, Yao J, Jin M, Yang S, Duong T. A novel improved cuckoo search algorithm for parameter estimation of photovoltaic (PV) models. Energies. 2018;11:1060.

[62] Abbassi A, Abbassi R, Heidari AA, Oliva D, Chen H, Habib A, Jemli M, Wang M. Parameters identification of photovoltaic cell models using enhanced exploratory salp chains-based approach. Energy 2020;198:117333.

[63] Qais MH, Hasanien HM, Alghuwainem S. Parameters extraction of three-diode photovoltaic model using computation and Harris Hawks optimization. Energy. 2020;195:117040.

[64] Elazab OS, Hasanien HM, Alsaidan I, Abdelaziz AY, Muyeen S. Parameter estimation of three diode photovoltaic model using grasshopper optimization algorithm. Energies. 2020;13:497.

[65] Long W, Wu T, Jiao J, Tang M, Xu M. Refraction-learning-based whale optimization algorithm for high-dimensional problems and parameter estimation of PV model. Eng Appl Artif Intell 2020;89:103457.

[66] Ridha HM, Gomes C, Hizam H. Estimation of photovoltaic module model's parameters using an improved electromagnetic-like algorithm. Neural Comput Appl 2020;32(16):12627–42.

[67] Messaoud RB. Extraction of uncertain parameters of single and double diode model of a photovoltaic panel using Salp Swarm algorithm. Measurement 2020;154:107446.

[68] Long W, Cai S, Jiao J, Xu M, Wu T. A new hybrid algorithm based on grey wolf optimizer and cuckoo search for parameter extraction of solar photovoltaic models. Energy Convers Manage 2020;203:112243.

[69] Chen X, Yu K. Hybridizing cuckoo search algorithm with biogeography-based optimization for estimating photovoltaic model parameters. Sol Energy 2019;180:192–206.

[70] Li S, Gong W, Yan X, Hu C, Bai D, Wang L, et al. Parameter extraction of photovoltaic models using an improved teaching-learning-based optimization. Energy Convers Manage 2019;186:293–305.

[71] Yu K, Qu B, Yue C, Ge S, Chen X, Liang J. A performance-guided JAYA algorithm for parameters identification of photovoltaic cell and module. Appl Energy 2019;237:241–57.

[72] Benkercha R, Moulahoum S, Taghezouit B. Extraction of the PV modules parameters with MPP estimation using the modified flower algorithm. Renewable Energy 2019;143:1698–709.

[73] Yu K, Liang J, Qu B, Cheng Z, Wang H. Multiple learning backtracking search algorithm for estimating parameters of photovoltaic models. Appl Energy 2018;226:408–22.

[74] Ram JP, Babu TS, Dragicevic T, Rajasekar N. A new hybrid bee pollinator flower pollination algorithm for solar PV parameter estimation. Energy Convers Manage 2017;135:463–76.

[75] Chen X, Yu K, Du W, Zhao W, Liu G. Parameters identification of solar cell models using generalized oppositional teaching learning based optimization. Energy. 2016;99:170–80.

[76] Niu Q, Zhang H, Li K. An improved TLBO with elite strategy for parameters identification of PEM fuel cell and solar cell models. Int J Hydrogen Energy 2014;39:3837–54.

[77] Gong W, Cai Z. Parameter extraction of solar cell models using repaired adaptive differential evolution. Sol Energy 2013;94:209–20.

[78] Jordehi AR. Time varying acceleration coefficients particle swarm optimisation (TVACPSO): A new optimisation algorithm for estimating parameters of PV cells and modules. Energy Convers Manage 2016;129:262–74.

[79] Muhsen DH, Ghazali AB, Khatib T, Abed IA. Parameters extraction of double diode photovoltaic module's model based on hybrid evolutionary algorithm. Energy Convers Manage 2015;105:552–61.

[80] Faramarzi A, Heidarinejad M, Mirjalili S, Gandomi AH. Marine Predators Algorithm: A nature-inspired metaheuristic. Expert Syst Appl 2020;152:113377.

[81] Nahla, M. Yahaya, N. Balbir. S. Single-Diode Model and Two-Diode Model of PV Modules: A Comparison. 2013 IEEE International Conference on Control System, Computing and Engineering, Penang; 2013.

[82] Oliva D, Abd El Aziz M, Hassanien AE. Parameter estimation of photovoltaic cells using an improved chaotic whale optimization algorithm. Appl Energy 2017;200:141–54.

[83] Ebrahimi SM, Salahshour E, Malekzadeh M, Gordillo F. Parameters identification of PV solar cells and modules using flexible particle swarm optimization algorithm. Energy. 2019;179:358–72.

[84] Mantegna RN. Fast, accurate algorithm for numerical simulation of Levy stable stochastic processes. Phys Rev E 1994;49:4677.

[85] Aydin, O. Gozde, H. Dursun, M. Taplamacioglu. M.C. Comparative Parameter Estimation of Single Diode PV-Cell Model by Using Sine-Cosine Algorithm and Whale Optimization Algorithm. 2019 6th International Conference on Electrical and Electronics Engineering (ICEEE). IEEE; 2019. pp. 65-8.

[86] Deotti, L.M.P. Pereira. J.L.R. Parameter Extraction of One-Diode Photovoltaic Model using Lévy Flight Directional Bat Algorithm. 2019 IEEE PES Innovative Smart Grid Technologies Conference-Latin America (ISGT Latin America). IEEE; 2019. pp. 1-6.

[87] Tong NT, Pora W. A parameter extraction technique exploiting intrinsic properties of solar cells. Appl Energy 2016;176:104–15.

[88] Elazab OS, Hasanien HM, Elgendy MA, Abdeen AM. Parameters estimation of single-and multiple-diode photovoltaic model using whale optimisation algorithm. IET Renew Power Gener 2018;12:1755–61.

[89] Tanabe, R. Fukunaga. A.S. Improving the search performance of SHADE using linear population size reduction. 2014 IEEE congress on evolutionary computation (CEC). IEEE; 2014. pp. 1658-65.

[90] Abdalla O, Rezk H, Ahmed EM. Wind driven optimization algorithm based global MPPT for PV system under non-uniform solar irradiance. Sol Energy 2019;180:429–44.

[91] Di Somma M, Graditi G, Heydarian-Forushani E, Shafie-Khah M, Siano P. Stochastic optimal scheduling of distributed energy resources with renewables considering economic and environmental aspects. Renewable Energy 2018;116:272–87.